Tectonophysics 909 (2025) 230788

Contents lists available at ScienceDirect

Tectonophysics

journal homepage: www.elsevier.com/locate/tecto

Azimuthally anisotropic Rayleigh-wave phase-velocity maps of Europe

Chiara Civiero [a,*], Raffaele Bonadio [b], Antonio Villaseñor [c]

[a] Department of Mathematics, Informatics and Geosciences, University of Trieste, Trieste, Italy
[b] Bullard Laboratories, Department of Earth Sciences, University of Cambridge, Cambridge CB30EZ, UK
[c] Institut de Ciències del Mar, ICM-CSIC, Barcelona, Spain

ARTICLE INFO

Keywords:
Ambient noise
Rayleigh waves
Phase-velocity maps
Azimuthal anisotropy
European lithosphere
Lithospheric structure

ABSTRACT

The European lithosphere is highly heterogeneous, with significant velocity contrasts across the continent. Despite its complexity, much of its detailed structure remains unexplored. We present azimuthally anisotropic phase-velocity maps of Rayleigh waves in the period range 4–40 s for Europe, derived from two years (2011−2012) of continuous waveform data from the Virtual European Broadband Seismic Network (VEBSN) and various temporary arrays. Using ambient-noise cross-correlation, we compute two-station dispersion measurements and integrate them into a tomographic inversion, simultaneously solving for isotropic and anisotropic structures through a least-squares approach. Our thorough suite of tests optimizes regularization and evaluates the resolution and trade-offs between isotropic and anisotropic anomalies. The phase-velocity maps at shorter periods reveal detailed images of major sedimentary basins, with the lowest velocities detected beneath the North German Basin, North Sea Basin, Rhone Basin, Po Plain, Pannonian Basin, and the Bay of Biscay. At longer periods, low-velocity anomalies are prominent beneath the Alps, Northern Apennines, Dinarides, and Anatolian Peninsula. Azimuthal anisotropy is also mapped in the shallow lithosphere, with fast axes in Southern Europe aligned parallel to mountain ranges such as the Pyrenees and Alpine-Apennine system. In Central Europe, the Tornquist-Teisseyre suture zone marks a transition between two domains of different anisotropic structures, suggesting "frozen-in" fabrics originated before the continental collision. The level of detail of these new phase-velocity maps makes them suitable for joint inversion with different types of geophysical data and as starting models for other imaging methods such as full-waveform inversion.

1. Introduction

Rayleigh and Love surface waves are well-suited for constraining the crustal and uppermost mantle structure of continents and oceans (Bensen et al., 2008; Ekström, 2011; Ritzwoller and Levshin, 1998). Because they propagate within the uppermost layers of the Earth, these waves typically are more sensitive to the shallow structure than body waves. Over the past two decades, surface-wave tomography using ambient seismic noise—commonly known as ambient-noise tomography (ANT)—has revolutionized seismic imaging across various scales by enabling the estimation of group and phase velocities (e.g., Bao et al., 2020; Bensen et al., 2009; Cho et al., 2007; Lin et al., 2013; Malory et al., 2022; Shapiro et al., 2005; Stehly et al., 2009).

Empirical Green's functions between two points can be estimated through the cross-correlation of the diffuse wavefield recorded at the two locations when noise sources are well distributed (Malcolm et al., 2004; Shapiro and Campillo, 2004; Snieder, 2004). This method excels at producing accurate 2D phase-velocity maps at different periods on regional and global scales. With high horizontal resolution (often 100 km or less, depending on interstation spacing), ANT-generated dispersion maps offer detailed insights into surface-wave behavior and are strongly correlated with underlying tectonic structures.

Surface waves sample varying depths based on their period, and phase velocity variations over a broad range can help constrain seismic anisotropy with depth (Montagner and Nataf, 1986). Azimuthal anisotropy affects the speed of seismic waves in the horizontal plane, causing directional dependence. In the upper crust, anisotropy is mainly due to aligned cracks or layering (shape-preferred orientation, SPO) from tectonic stress (Crampin and Peacock, 2008; McNamara and Owens, 1993), while in the middle-to-lower crust, it arises from strain-induced lattice preferred orientation (LPO) of minerals like amphibole (Barruol and Mainprice, 1993; Lloyd et al., 2009). In the upper mantle, LPO of minerals, particularly olivine, is the dominant source of anisotropy (Zhang and Karato, 1995). These anisotropic patterns can result

* Corresponding author.
E-mail address: chiara.civiero@units.it (C. Civiero).

https://doi.org/10.1016/j.tecto.2025.230788
Received 21 November 2024; Received in revised form 5 May 2025; Accepted 12 May 2025
Available online 13 May 2025
0040-1951/© 2025 The Authors. Published by Elsevier B.V. This is an open access article under the CC BY license (http://creativecommons.org/licenses/by/4.0/).

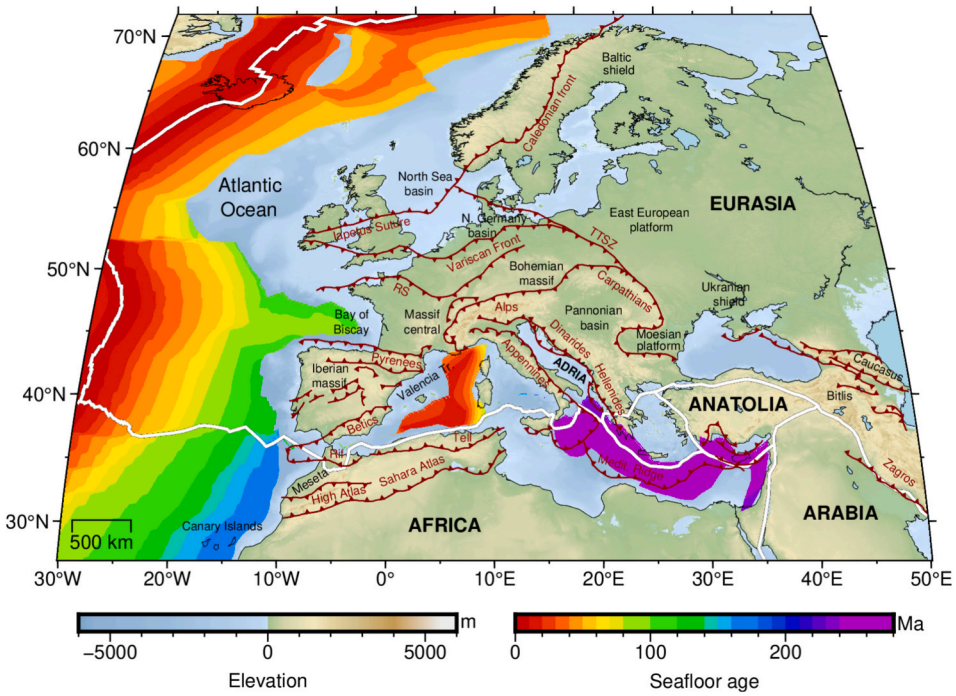

Fig. 1. Simplified tectonic map of the European region. Brown lines with filled ticks denote the main orogenic frontal zones. The names of the orogens and sutures are indicated in brown, and the names of the other features are in black. TTSZ: Tornquist-Teisseyre Suture Zone, RS: Rheic Suture. Plate boundaries from Bird (2003) are shown in white. The age of the oceanic lithosphere derived from magnetic and other geophysical data is taken from (Müller et al., 2008). (For interpretation of the references to colour in this figure legend, the reader is referred to the web version of this article.)

from both past and ongoing deformation processes within the lithosphere and are influenced by absolute plate motions. Also, seismic anisotropy measurements may provide new constraints on mantle circulation patterns, as olivine-rich aggregates cause the a-axes of olivine crystals to align with the direction of mantle flow (Ribe, 1989). Examining the strength and orientation of fast anisotropic directions provides key insights into historical and present-day deformation in the crust and upper mantle (e.g., Babuska and Cara, 1991; Crampin, 1984; Long and Silver, 2008; Vinnik et al., 1992).

The European continent features a complex tectonic setting, largely driven by the convergence of the Eurasian and African plates. This compression led to the closure and subduction of the Tethys Ocean, forming fragmented plate boundaries and arcuate mountain belts such as the Alps, Pyrenees, Apennines, Dinarides, Hellenides, and Carpathians (Dewey et al., 1989). Backarc extension in regions like the Algero-Provençal Sea, Tyrrhenian Sea, Pannonian Basin, and Aegean Sea resulted from oceanic lithosphere subduction, with slab rollback and trench retreat still active under the Calabrian and Hellenic Arcs (Wortel and Spakman, 2000). In the Eastern Mediterranean, the Arabian Plate's northward movement results in collision with Eurasia, contributing to the counterclockwise rotation of the Anatolian block (Le Pichon et al., 1995). To the north, the East European Craton (EEC), including the Baltic and Ukrainian Shields and the East European Platform, represents a stable Precambrian region. The Tornquist-Tesseyre Suture Zone (TTSZ) marks its transition to Phanerozoic Europe to the west (Zielhuis and Nolet, 1994). During the Paleozoic, Central and Western Europe were mainly shaped by the Caledonian and Variscan orogenies, creating mountain belts currently distributed along the western coast of Scandinavia, the British Isles, Germany, and France (Pharaoh, 1999). Further south, the European Rift System has been associated with extension during the Cenozoic. This activity has played a role in the development of structures such as the Massif Central, the Rhine Graben, and the Eifel region, where the origin of the rift-related volcanism may involve both passive and active processes, potentially including plume-related contributions (e.g., Goes et al., 1999; Michon et al., 2003; Ziegler, 1992). Key tectonic structures, including sedimentary basins, mountain ranges, and sutures, are shown in Fig. 1.

A significant number of surface-wave tomographic studies at different scales focus on constraining the driving forces of the tectonic processes occurring in the European lithosphere (e.g., El-Sharkawy et al., 2020; Legendre et al., 2012; Lu et al., 2018; Meier et al., 2016; Nita et al., 2016; Panza and Mueller, 1980; Ritzwoller and Levshin, 1998; Soomro et al., 2016; Zhu and Tromp, 2013). However, the fine-scale seismic structure remains inconsistently resolved in some parts of the continent due to a lack of data and thus a broader scale picture is missing. The rapid growth of seismic experiments across all of Europe has yielded a significant increase in the sampling making this region an excellent laboratory to search for contributions of lithospheric deformation and hence to improve the understanding of the tectonic evolution of the region.

In this study, we use seismic ambient noise phase dispersion data from a dense network of stations across Europe to produce azimuthally anisotropic Rayleigh-wave phase-velocity maps for the crust and uppermost mantle. Our new maps show a strong correlation between shear-wave speeds and major geological features of the continent. The fast orientations of seismic anisotropy reveal a complex pattern, influenced by regional tectonics, with notable differences from southern to northern Europe. By mapping lateral changes of anisotropy, we are able to constrain lithospheric blocks with different orientations of fabrics and identify domain boundaries and sutures.

2. Seismic data and method

2.1. Data processing and phase-velocity measurements

In this study, we use data from 831 seismic stations, including both permanent stations from the Virtual European Broadband Seismic Network (VEBSN) (Van Eck et al., 2004) and temporary stations from various experiments such as IberArray (Díaz et al., 2009), PICASSO (Platt et al., 2008), WILAS (Custódio et al., 2014), and PYROPE (Chevrot

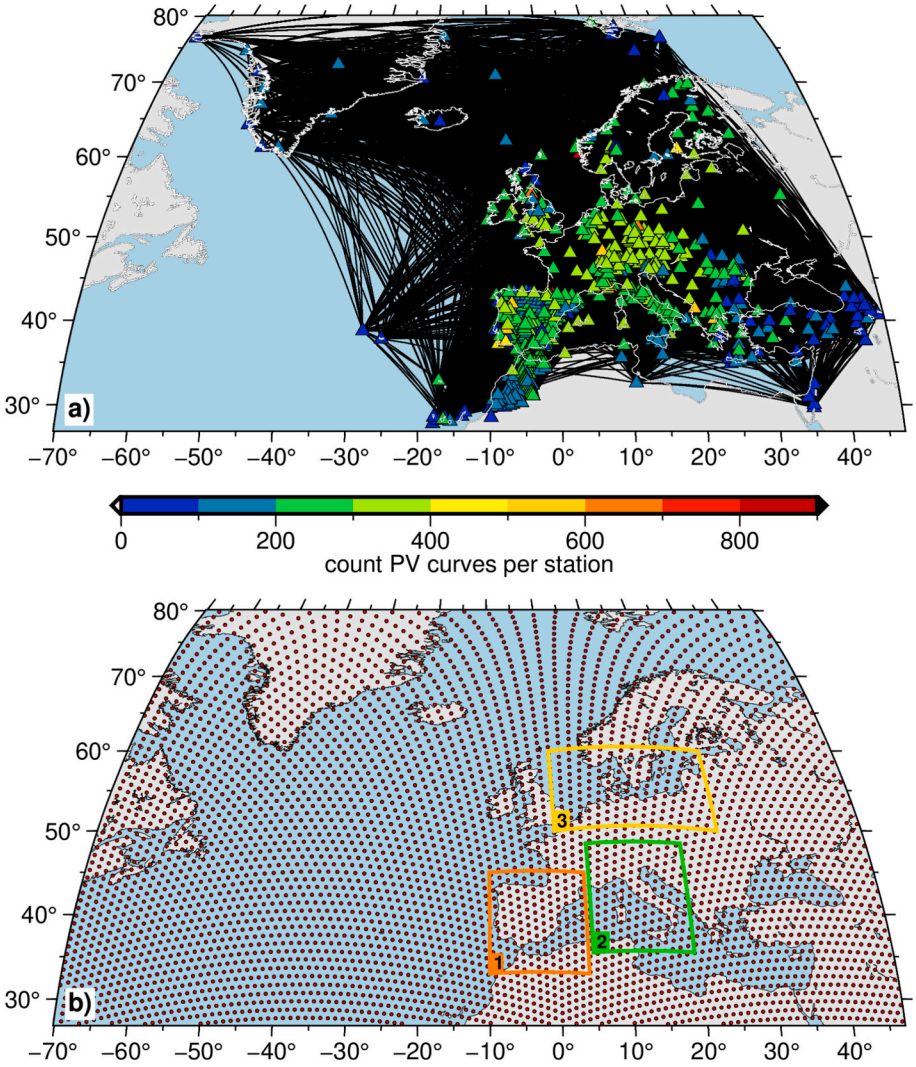

Fig. 2. a) Map of seismic stations used in this study colour-coded according to the number of phase-velocity dispersion curves; b) map of the triangular grid knot points used to parametrize the tomographic inversion. The key regions where we focus our interpretation are indicated with boxes of different colors: 1. orange, the Iberian Peninsula; 2. green, the Alpine-Apennines region; 3. yellow, North-Central Europe. (For interpretation of the references to colour in this figure legend, the reader is referred to the web version of this article.)

et al., 2014). The dataset covers a period of 24 months between 2011 and 2012 (Fig. 2). Detailed station information, including network codes, station names, and coordinates, can be found in Table T1 of the Supporting Information. This results in dense regional coverage, although the path lengths between station pairs are highly variable, ranging from under a kilometer to over 10,000 km.

We process continuous vertical-component seismic data using the well-established ANT approach (Bensen et al., 2007; Shapiro et al., 2005), which is briefly summarized here. Prior to the correlations, we apply standard pre-processing to the continuous data that includes eliminating the mean and trend, removing the instrument response, applying a zero-phase bandpass filter between 1 and 150 s, converting the data to displacement, and downsampling them to 1 Hz. Cross-correlation is performed in the frequency domain using 4-h windows. After stacking the cross-correlograms for each station pair, we average the causal and acausal parts, which can be interpreted as the Rayleigh-wave component of the empirical Green's function, under the assumption that ambient noise wavefields are random and uniformly distributed (Lin et al., 2008; Udías, 2009).

The phase velocity dispersion of the fundamental Rayleigh mode for each stacked cross-correlogram is extracted using the multiple-filter technique (e.g., Meier et al., 2004), carried out using an automated implementation frequency-time analysis (FTAN), followed by strict quality control (Bensen et al., 2007). The automated procedure, applied to all station pairs, measures dispersion between 2 and 100 s. However, we then pick up dispersion measurements between 4 and 40 s, as this is the period range in which the signal-to-noise ratio (SNR) is large enough to be considered reliable (Lin et al., 2008; Ritzwoller and Levshin, 1998). Only cross-correlations with an SNR > 10 are retained. Dispersion measurements with interstation spacing of less than 3 complete wavelengths at each period are discarded. The number of measurements for each period is shown in Fig. 3. The azimuthal path coverage is comprehensive except near the edges of the study area.

2.2. Inversion for Rayleigh-wave phase-velocity maps

The dispersion curves for the 84,380 interstation paths and their average are calculated at each period, and the results are shown in Fig. 3. The average dispersion curve lies below that derived from the global reference model AK135 (Kennett et al., 1995) for all periods and also below PREM (Dziewonski and Anderson, 1981) from ~12 to 40 s.

After deriving the dispersion measurements, we then invert them for both isotropic and anisotropic (2ψ and 4ψ components) Rayleigh-wave phase-velocity maps, all parameterized at the knots of the same

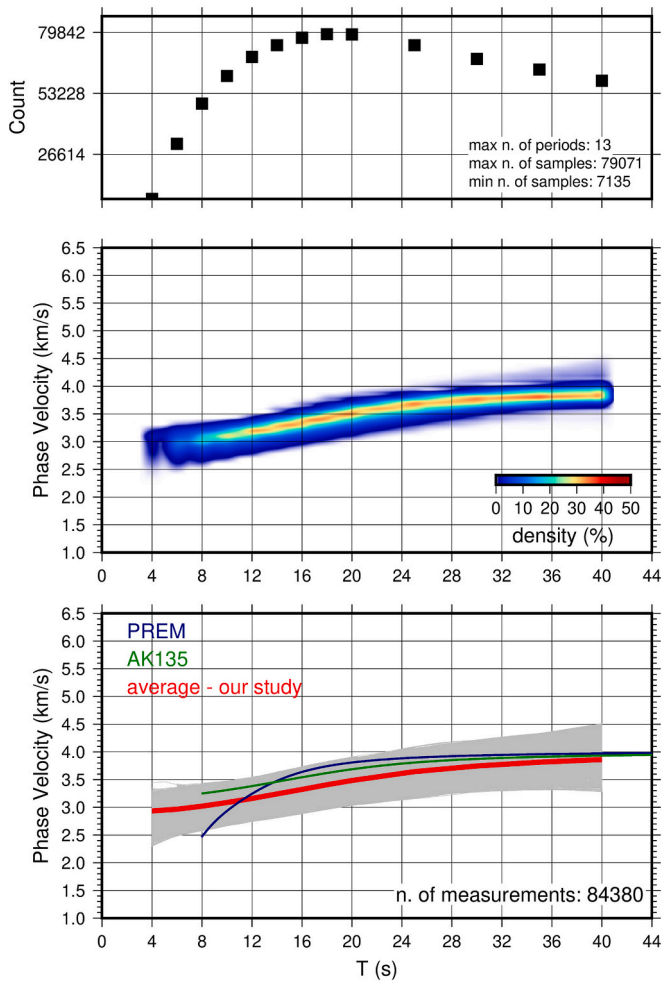

Fig. 3. Upper panel: number of measurements at each period (4, 6, 8, 10, 12, 14, 16, 18, 20, 25, 30, 35, and 40 s). Middle panel: density distribution of the total dispersion curves. Bottom panel: All the dispersion curves computed (grey) and the average curve (red) in the period range 4–40 s. Light blue and dark green lines show the PREM and AK135 reference curves, respectively. (For interpretation of the references to colour in this figure legend, the reader is referred to the web version of this article.)

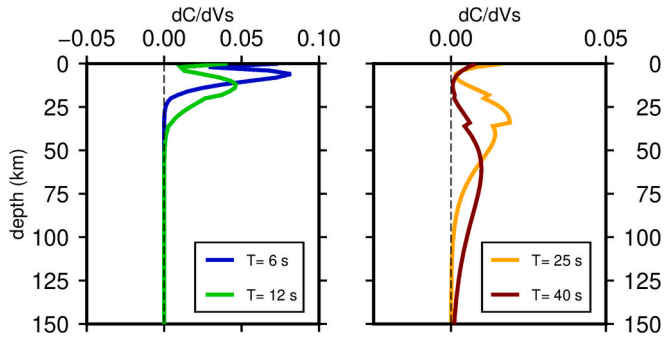

Fig. 4. Depth sensitivity kernels of surface waves at four periods (6, 12, 25, and 40 s). The sensitivity curves are the Fréchet derivatives of the phase velocities of the fundamental-mode Rayleigh phase waves with respect to S-wave velocities.

triangular grid with a nearly-uniform spacing of around 100 km (Fig. 2b). The inter-station dispersion measurements from cross-correlations are used to invert for the Rayleigh-wave phase-velocity maps using the method described in Darbyshire and Lebedev (2009). The inversion was performed using the LSQR algorithm of Paige and Saunders (1982), applying smoothing and slight norm damping (Lebedev and Van Der Hilst, 2008; Zhang et al., 2009). The effect of smoothing is illustrated in Figs. S1-S3 for three highly sampled regions in Europe (Iberia, the Italian Peninsula, and North-Central Europe). With minimal smoothing, the model is dominated by noise due to insufficient data coverage to resolve small-scale structures. Conversely, applying extremely strong smoothing eliminates lateral structural heterogeneities. A moderately strong degree of smoothing is then chosen for the isotropic component. Anisotropy patterns can be reliably resolved only at spatial scales larger than those of isotropic heterogeneity (Darbyshire and Lebedev, 2009; Polat et al., 2012). Consequently, both the 2ψ and 4ψ anisotropy patterns were smoothed more strongly than the isotropic phase-velocity variations. In order to minimize the impact of errors in the measurements on phase-velocity maps, we exploit the data redundancy of the dataset and select only the mutually consistent data through an *a–posteriori* outlier rejection procedure. At every period, we use the first-iteration phase-velocity map to compute synthetic data. We then compare the synthetic and real data and discard the measurements with the largest misfit. In our study, we keep a selected, most mutually consistent 70 % of the initial dataset and compute the final phase-velocity maps with these "de-noised" data.

Depth resolution is controlled by the sensitivity kernels of the Rayleigh waves, which suggests that the period range covered by our measurements (4–40 s) corresponds approximately to a depth range that spans the crust and shallow upper mantle (Fig. 4). At the shortest periods (<10 s), phase velocities are primarily sensitive to shear velocities at shallow depths (sedimentary basins and upper crust). As the seismic velocities in the sediments are low, short-period low-velocity anomalies are a good indicator of sedimentary basins. At longer periods (25–40 s), Rayleigh waves sample both the lower crust and uppermost mantle. The phase velocities in this range vary approximately inversely with the crustal thickness (high velocities in regions with a thin crust and low velocities in regions with a thick crust).

Data coverage is not uniform across the continent. To visualize the coverage, we use the sums of the columns of the sensitivity matrix (in percentage). The column sums reflect, for each grid node, the amount of data sampling each model parameter (Bonadio et al., 2021). Data coverage is shown in Fig. 5 for the 6, 10, 14, 20, 25, 30, 35, and 40 s measurements and is highest in Western and Central Europe whereas it gradually degrades, as expected, towards the edges of the study region.

3. Resolution analysis

The resolution of isotropic velocity variations is tested using a series of synthetic models with the attempt to recover the structure using the path distribution of the whole European dataset. The NE–SW gradient in isotropic phase velocity over the study region is retrieved to a satisfactory level (Supplementary Fig. S4) with the transition from slow (red shade) to fast velocities (blue shade) occurring in the correct location. The amplitude recovery of velocity anomalies is generally good. Resolution is better in Western Europe compared to the northeastern part of the continent.

We then run a spike test using 14 negative anomalies of amplitude −2.5 % distributed across Europe (Fig. 6). The ability to recover spike patterns varies based on their position relative to areas with dense or sparse path coverage. Most anomaly patterns are well-resolved, particularly in Western and Central Europe. For example, the spikes in Eastern Europe and Iceland are largely poorly resolved as the path coverage is not particularly dense. This test indicates that the path coverage and the parameterization of the inversion are sufficient to provide an adequate recovery of phase-velocity anomalies of ~150–200 km in width across most of the study area.

To investigate the degree of leakage between isotropic and anisotropic heterogeneities in the models, we took the phase-velocity maps derived from our surface-wave dataset, we rotated the 2ψ anisotropy bars through 90° putting the 4ψ anisotropy values to zero and we then

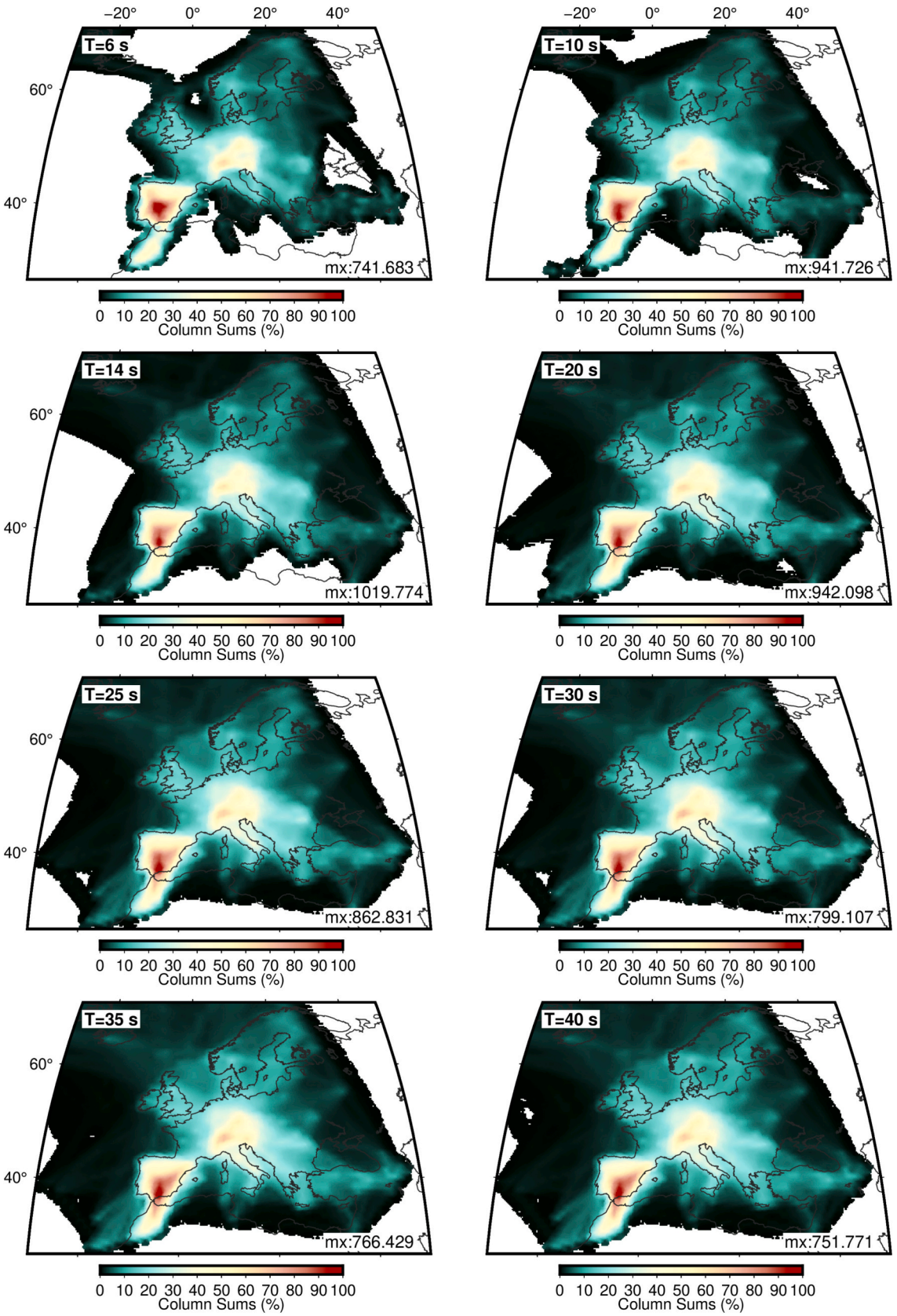

Fig. 5. Plot of the sums of the columns of the sensitivity matrix at six selected periods (6, 10, 16, 20, 30, 35, and 40 s). Dark green regions indicate zero sampling while dark red regions represent the most sampled regions. Column sums are a-dimensional; here they are plotted in percentage with respect to the maximum value at each period. (For interpretation of the references to colour in this figure legend, the reader is referred to the web version of this article.)

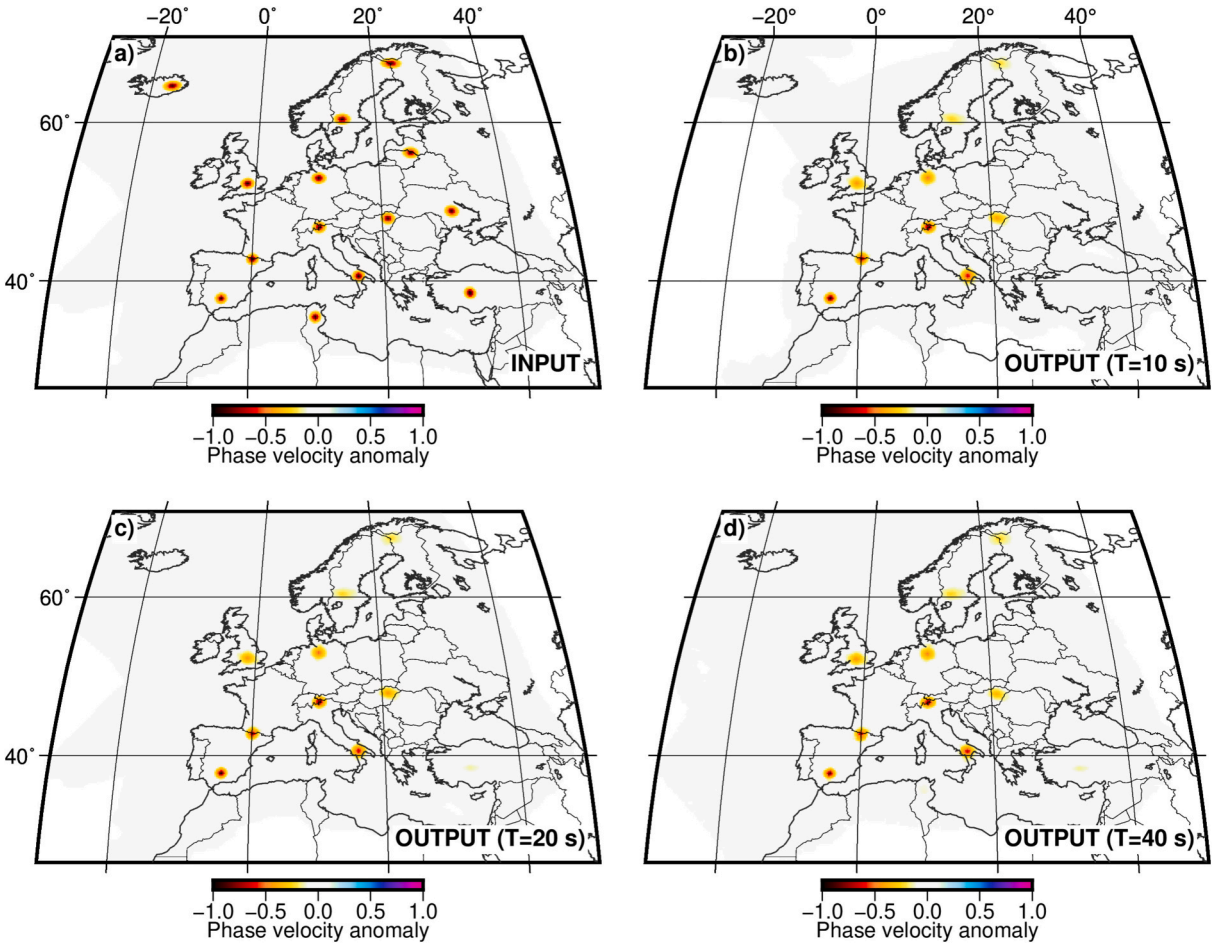

Fig. 6. Resolution tests for isotropic low-velocity spike anomalies placed in 14 different regions of Europe. The magnitude of the spikes has been normalized. No random noise has been added to the synthetic dataset. Panel a) shows the input spikes; panels b), c), and d) are the output spike anomalies at 10, 20, and 40 s, respectively. Note that the resolution is higher in Western and Central Europe compared to the eastern part of the continent where the coverage is decreased.

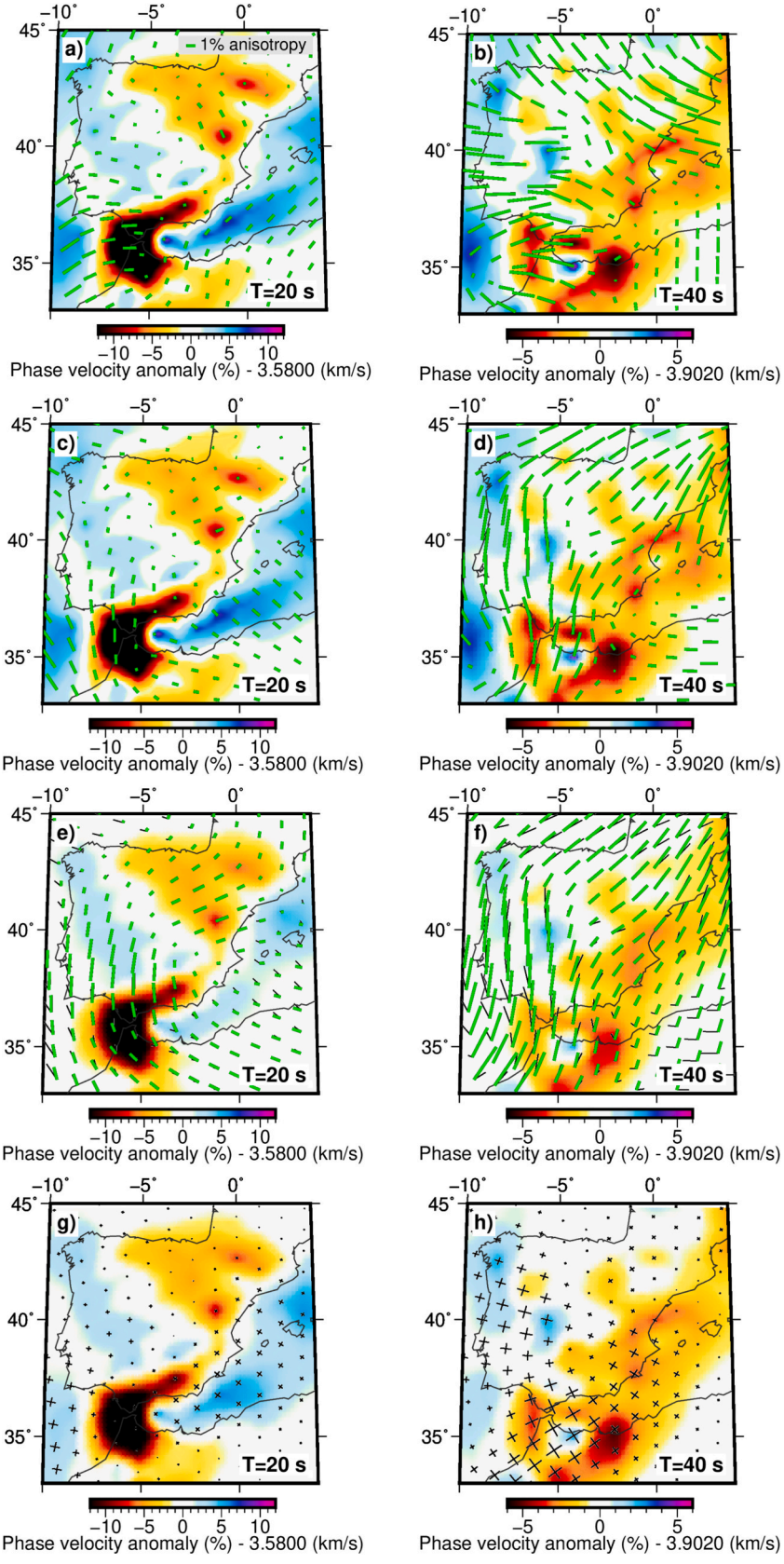

(caption on next page)

Fig. 7. Results of anisotropy leakage test focused on Iberia in which the starting model is taken from the original phase-velocity map but with 2ψ anisotropy directions rotated by 90° and 4ψ anisotropy set to zero. The anisotropy is plotted with green sticks. (a) Original phase-velocity map at 20 s; (b) Original phase-velocity map at 40 s; (c) map at 20 s with rotated anisotropy used as input; (d) map at 40 s with rotated anisotropy used as input; (e) and (f) results of inversion for isotropic phase velocity plus 2ψ anisotropy values at 20 s (e) and 40 s (f). The input anisotropy sticks are plotted with a thinner black line below the output anisotropy values; (g) and (h) results of inversion for isotropic phase velocity plus 4ψ anisotropy values at 20 s (g) and 40 s (h). (For interpretation of the references to colour in this figure legend, the reader is referred to the web version of this article.)

re-inverted the resulting synthetic model. A noticeable shift in the fast direction of the recovered model would suggest that the original dataset had unacceptable leakage between isotropic and anisotropic anomalies, or that spurious anisotropy was introduced due to path biases. We show the results of the test in Figs. 7–9 (the same sub-regions used before to investigate the effect of smoothing). The output images indicate a good recovery of the fast directions of the rotated 2ψ anisotropy bars and some leakage into 4ψ anisotropy, in particular on the edges of the three regions, such as the Mediterranean Sea (Figs. 7 and 8), Atlantic Ocean (Fig. 7) and towards Eastern Europe (Fig. 9). The amplitude observed in the spurious 4ψ anisotropy output has an average of 0.016 km/s for $T = 20$ s and 0.013 km/s for $T = 40$ s compared to 2ψ averaging 0.022 km/s and 0.017 km/s, respectively. The test shows that the mapped fast directions of anisotropy are robust in most of the continental domain.

Overall, these tests confirm that the resolution of phase-velocity anomalies and azimuthal anisotropy is robust across much of Europe, though some leakage occurs close to the model's borders.

4. Preferred tomographic model

Lateral phase-velocity variations at different periods reflect structural heterogeneity within the lithosphere across the continent (Fig. 10). Overall, the inversions reveal the same dominant regional velocity anomalies as previous tomography studies (e.g., El-Sharkawy et al., 2024; El-Sharkawy et al., 2020; Lu et al., 2018; Nita et al., 2016; Soomro et al., 2016; Verbeke et al., 2012), confirming that our data samples these patterns accurately. Notably, the model consistently images key features observed in earlier studies, including prominent low-velocity anomalies beneath the Gibraltar Arc System and major orogenic belts such as the Alps-Apennines, Dinarides, Hellenides, and Carpathians. Additionally, the high-velocity anomaly beneath the Ligurian/Tyrrhenian Sea is clearly reproduced. Our phase-velocity maps also reveal low-velocity anomalies beneath the Anatolian Plateau at periods greater than 15 s, in agreement with previously published models. These correspondences underscore the robustness of our inversion approach and its capability to accurately reflect regional tectonic structures. Nevertheless, the increase in the data sampling allows us to better constrain the pattern of the isotropic variations due to the higher resolution of the lithospheric structure beneath Western and Central Europe. To guide assessment, Fig. 11 shows a map of sediment thickness and crustal thickness CRUST1.0 (Laske et al., 2013) and the LAB depth taken from the global model of Fullea et al. (2021). We include the thickness of the sediments and the crust from the model EuCRUST-07 (Tesauro et al., 2008) in Supplementary Fig. S5 to see if our surface-wave tomography is consistent with the integrated results from seismic reflection, refraction, and receiver function studies. We also show in Supplementary Fig. S6 the LAB depths at 18 discrete locations, recently determined through thermochemical inversion using Rayleigh and Love wave phase velocities, heat flow, rock densities, and thermochemical conditions (El-Sharkawy et al., 2024).

In the Western Mediterranean, the most prominent low-velocity features at short periods (4 to 20 s) are associated with the Guadalquivir Basin (SE Spain), the flysch units of the Gibraltar Strait, and the thick sediment layer of the Gulf of Cadiz. Figs. 11A and S5A provide a comparison with sedimentary cover maps. High-velocity anomalies are imaged beneath Western Iberia, the Moroccan Meseta, and the Western Alboran Sea, in line with the fast velocities found in many tomography models of the Ibero-Maghrebian crust (Arroucau et al., 2021; Pedreira et al., 2003; Souriau et al., 2008). Moving towards Central Europe, strong low-velocity anomalies at the shortest periods are linked to sedimentary basins like the Paris Basin (Northern France), the North Sea and North German Basins (Germany and offshore), the Pannonian Basin (Hungary, Slovakia), the Po Basin (Northern Italy), the Rhone Basin (Southern France), and the Adriatic Sea. At longer periods (25 to 40 s), velocities become increasingly sensitive to crustal thicknesses. The phase-velocity maps exhibit prominent low-velocity anomalies beneath the orogens including the Betics, the Cantabrian-Pyrenees, the Alps, the Apennines, the Carpathians, the Dinarides, and the Hellenides. These features are due to the deeper crustal roots beneath mountain chains reaching depths of over 50 km (Fig. 11B and Fig. S5, Tesauro et al., 2008). Anatolia, at the edge of our resolved domain, shows very strong low-velocity anomalies at long periods, suggesting higher than usual temperatures. This is consistent with the flow of hot asthenospheric material coming from the Afro-Arabian rift system (Civiero et al., 2023; Civiero et al., 2022) and channeling through corridors where the lithosphere is thinned (70–80 km; Fullea et al., 2021; see Fig. 11C, or 60–70 km; El-Sharkawy et al., 2024; see Fig. S6). To the north-west, at the longest periods (>30 s) small-scale low-velocity anomalies are visible in areas with Cenozoic volcanic centres, such as those above the Eifel Hotspot and the Pannonian Basin (Wilson and Downes, 2006). These anomalies correspond to a shallow asthenosphere, with the LAB depth being less than 80 km and 60 km, respectively (see Fig. 11C and Fig. S6). Low velocities are also imaged below Iceland, probably associated with the presence of mantle material upwelling from deeper depths (e.g., Celli et al., 2021), with the LAB being located at depths shallower than 80 km. The abrupt change in Rayleigh wave velocity from negative to positive anomalies in the eastern part of the 30–40 s phase-velocity maps is associated with a change in lithospheric properties of the East European Platform and Baltic Shield. These regions are characterized by a cold, depleted cratonic lithosphere that extends beyond the maximum depth resolution of the surface waves in this study, with the LAB reaching depths greater than 180 km (see two locations of the Platform in Fig. S6), and in certain areas, exceeding 200 km (Fig. 11).

In summary, our maps reveal clear regional variations in phase velocities across Europe, with prominent low-velocity anomalies correlating with sedimentary basins and orogenic belts. The deeper lithospheric structures, such as thickened crust in mountain chains and hot asthenospheric material beneath thin-lithosphere corridors, are well constrained, offering new insights into the tectonic evolution of these regions.

5. Azimuthally anisotropic structures

In response to shear strain, crustal and mantle minerals can develop some specific fabrics that result in seismic anisotropy (Mainprice et al., 2010; Ribe, 1992). The direction of fast propagation is interpreted as the direction of maximum deformation (Christensen, 1984). The intrinsic anisotropy can be mapped seismically, from the azimuthal and polarization dependence of wave speeds. Here, we estimate and discuss the azimuth and the amplitude of the fast directions of anisotropy using the computed Rayleigh phase-velocity curves with the aim of examining the dominant, region-scale patterns of deformation. We show the anisotropic maps of all Europe in Fig. 12. To better discriminate between a possible coupling between the anisotropy and the stress field, we also provide the map of the stress field in Europe in Supplementary Fig. S7 taken from the World Stress Map (WSM) compilation (Heidbach et al.,

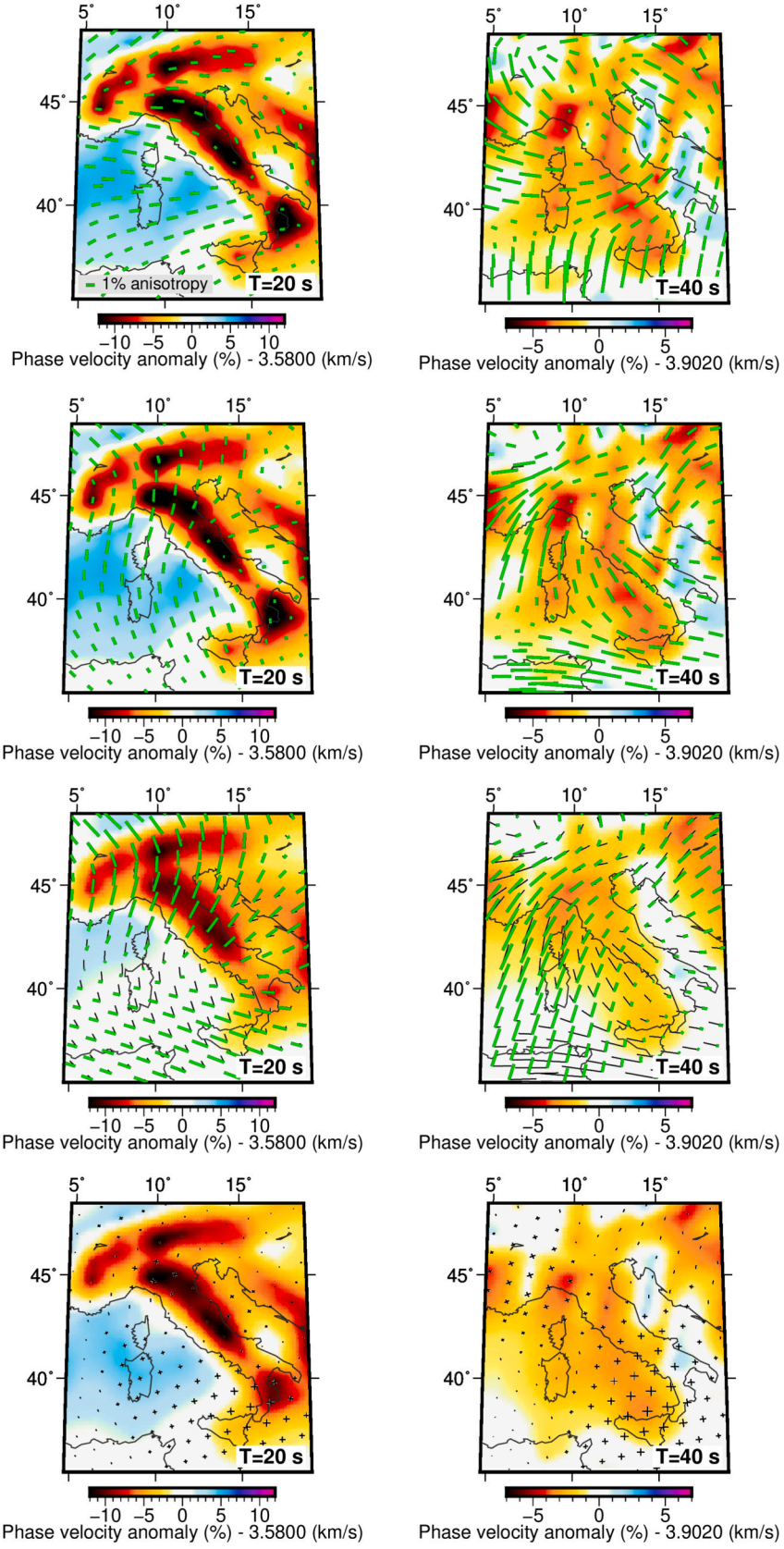

Fig. 8. Same as Fig. 7 but focused on the Italian Peninsula and Alpine region.

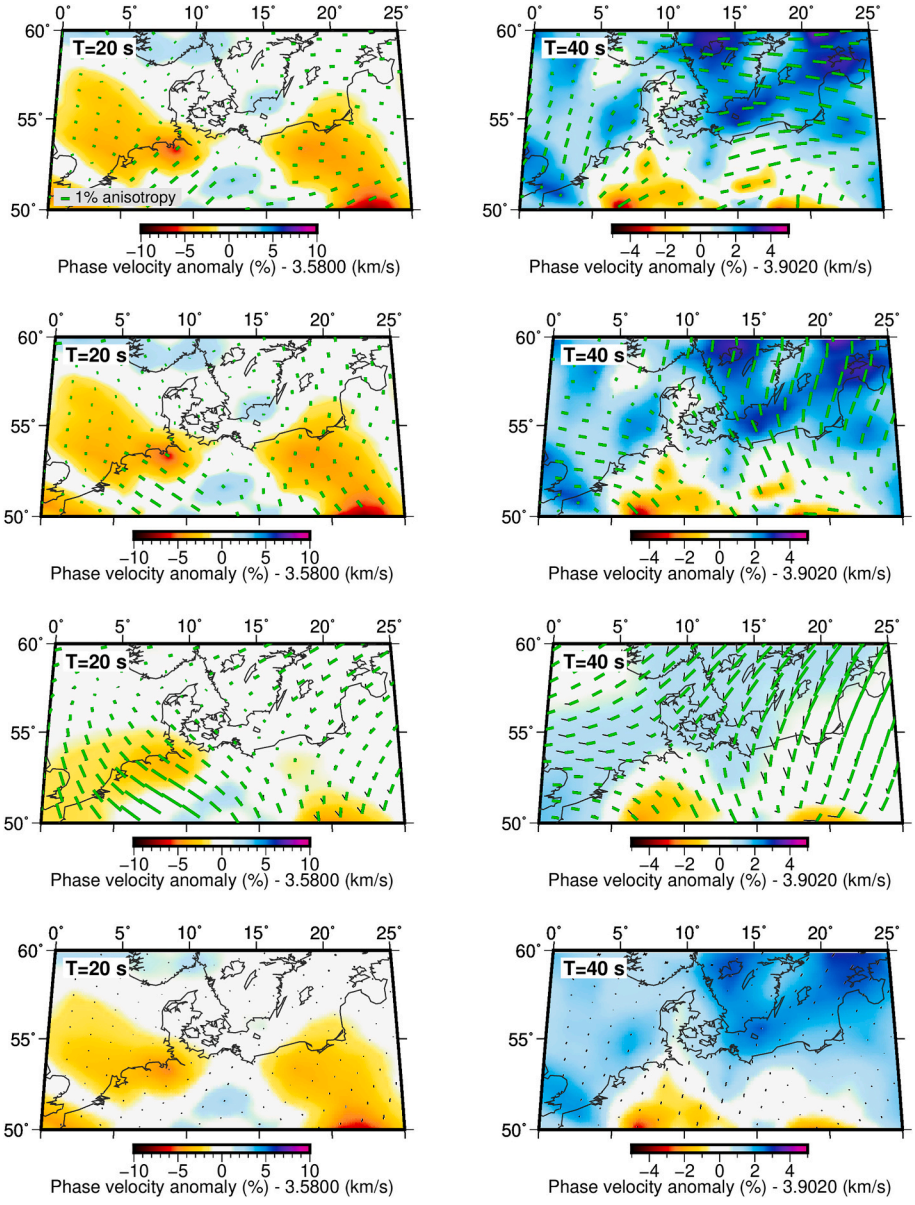

Fig. 9. Same as Fig. 7 but focused on North-Central Europe.

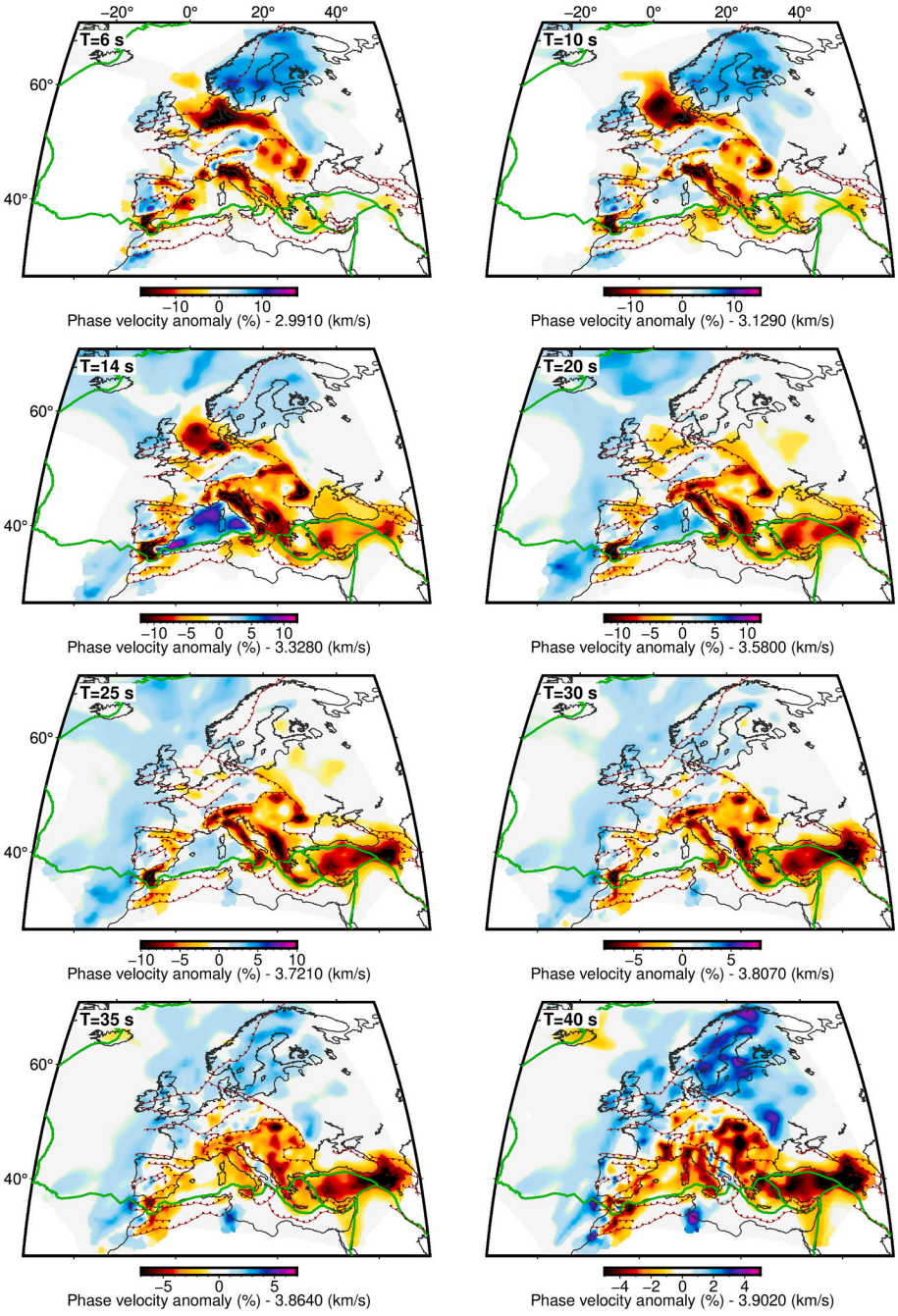

Fig. 10. Phase-velocity maps at six selected periods (same periods as in Fig. 5). The orogenic frontal zones are plotted in brown. Plate boundaries are shown in green. (For interpretation of the references to colour in this figure legend, the reader is referred to the web version of this article.)

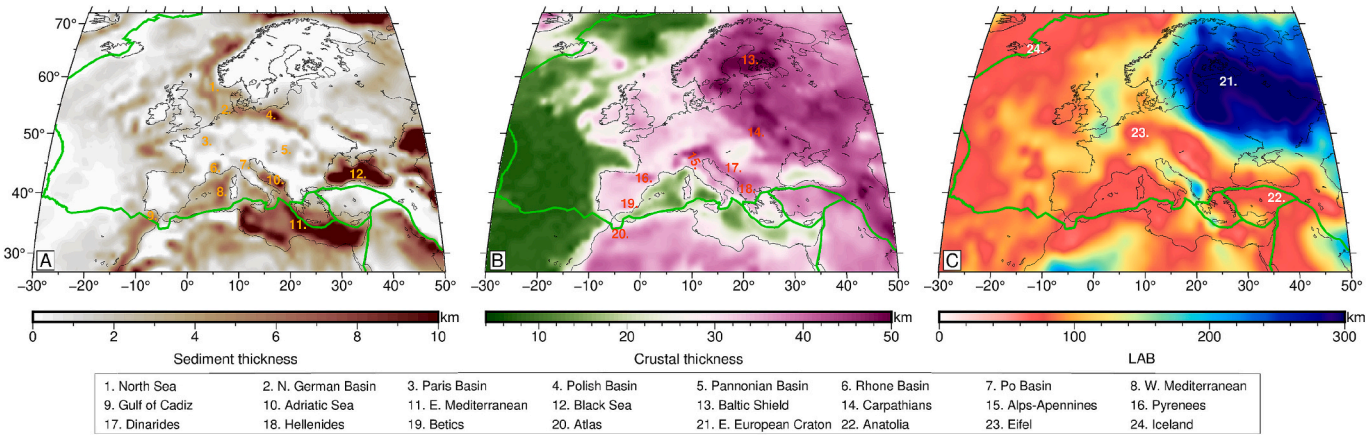

Fig. 11. Maps of the sediment thickness taken from CRUST1.0 (A), crustal thickness from CRUST1.0 (Laske et al., 2013) (B), and LAB depth (C) from the WINTERC-G model (Fullea et al., 2021) of Europe. Plate boundaries are shown in green. The locations of geological units discussed in the text are marked with numbers in each panel. (For interpretation of the references to colour in this figure legend, the reader is referred to the web version of this article.)

2018). Overall, we found that our anisotropic patterns, in particular beneath the Euro-Mediterranean region, are in good agreement with those imaged at the continental scale in previous shear-wave splitting analyses (e.g, Link and Rümpker, 2023; Schmid et al., 2004; Wüstefeld et al., 2009) and tomography models (Becker et al., 2012; Díaz et al., 2013; Nita et al., 2016; Zhu and Tromp, 2013). Specifically, our findings mirror previously reported features such as the orogen-parallel anisotropy beneath the Alps and Apennines (Díaz et al., 2013; Link and Rümpker, 2023), the anisotropic patterns beneath the Pyrenees (Nita et al., 2016; Díaz et al., 2013), and the W–E oriented anisotropy surrounding the Gibraltar slab (Díaz et al., 2013). These consistent observations further validate the reliability of our model in capturing the complex anisotropic characteristics of the region. It is important to note here that the current phase velocity maps primarily sample structure and anisotropy to uppermost mantle depths, while shear-wave splitting measurements integrate anisotropy from the core-mantle boundary to the surface, often representing the combined effects of the crust, lithospheric mantle, and asthenosphere. The good agreement observed between the shear-wave splitting measurements and our results may reflect similar uppermost-mantle processes but may not fully capture deeper anisotropic features that the shear-wave splitting data do.

Although robust anisotropy patterns are observed across the continent, we focus on three sub-regions (shown in Fig. 2b) where data sampling is highest. These regions have also been carefully tested for leakage between isotropic and anisotropic phase-velocity heterogeneities (see Figs. 7–9): 1) the Iberian Peninsula; 2) the Alpine-Apennines system; and 3) North-Central Europe. In particular, we assess if the fast directions of anisotropy –and, by inference, the frozen-in directions of shear– are parallel to ancient sutures or reflect simple shear observed today in tectonically active regions.

5.1. Iberian Peninsula

Iberia is the far western end of the Alpine orogenic belt. To the north of the peninsula, the Pyrenean-Cantabrian range marks the tectonic boundary between Eurasia and Iberia. This mountain range was built at ~84 Ma as the result of the convergence between the African and Eurasian plates and involved the inversion of pre-existing rift zones (Teixell et al., 2018). Continued African-Eurasian compression transmitted the plate margin stress fields towards the interior and created the Iberian Chain, oriented NW–SE. The Iberian Massif, in the western half of Iberia, is the result of the Variscan orogeny during the Devonian and Carboniferous (Gibbons and Moreno, 2002). Further south, the Betic-Rif belt constitutes the westernmost end of the Alpine orogeny. It comprises the Gibraltar Arc and surrounds the extensional Alboran Basin. In between the Alpine orogens, four foreland basins filled with a thick sedimentary cover –the Ebro, Duero, Tajo, and Guadalquivir Basins– are formed (Vergés and Fernàndez, 2012).

The Iberian Peninsula has been the target of several surface-wave investigations. Using two-station dispersion measurements, Corchete et al. (1995) obtained the first shear-wave model of the Iberian lithosphere and asthenosphere. The shallow structure has also been studied using short-period Rayleigh waves from small earthquakes and explosions for different parts of Iberia (Chourak et al., 2005). Villaseñor et al. (2007) computed group-velocity maps of Rayleigh waves at periods from 8 to 25 s across the peninsula, which reveal the main structural elements of the Iberian upper crust, including the Iberian Massif, Alpine orogens, and major sedimentary basins. The subsequent models of the Iberian lithospheric structure tend to converge on the distribution of the isotropic heterogeneities below the peninsula (e.g., Corchete and Chourak, 2011; Feng and Diaz, 2023; Macquet et al., 2014; Palomeras Thurner et al., 2014; Palomeras et al., 2017; Silveira et al., 2022; Silveira et al., 2013). Surface-wave studies on seismic anisotropy are fewer and often limited to a relatively small region (e.g., Acevedo et al., 2020; Marone et al., 2004; Paulssen et al., 1990). Feng and Díaz (2022) revealed that fast directions of anisotropy align parallel to the strike of the mountain belts in the crust and are predominantly close to E–W at lithospheric mantle depths in the rest of the peninsula.

In our azimuthally anisotropic phase-velocity maps, the fast directions align sub-parallel to the strike of the Pyrenees and the Cantabrian Mountains (and to the Hercynian preexisting faults) at the shortest periods shifting to a more northerly orientation at periods >25 s (Fig. 13). These patterns suggest the presence of a layer of anisotropy primarily related to frozen-in structures in the shallow crust (e.g., extensional shearing related to the opening of the Bay of Biscay) and an additional weak anisotropic layer below, which does not align with surface features and may be related to a previous stage of the collision during the Variscan orogeny. Also, as observed by Acevedo et al. (2020), the NW–SE oriented fast directions in the western Cantabrian belt may depict the trend of the main Variscan thrusts in the area.

In the Betics, weak anisotropy is observed at periods <20 s with fast directions following the topography of the belt until the Strait of Gibraltar. However, no clear evidence of anisotropy is seen at longer periods beneath the belt. Anisotropy is stronger offshore, in the western part of the Alboran Sea and between the Balearic Islands and the coast of Africa. Here, the fast directions are in a NE–SW orientation similar to what was found by Díaz et al. (2013), likely reflecting the westward escape of the Alboran block and its extension-related tectonics (Alpert et al., 2013). In line with Feng and Díaz (2022), the anisotropy in the Gibraltar Arc System is strong, with fast directions mostly in the W–E

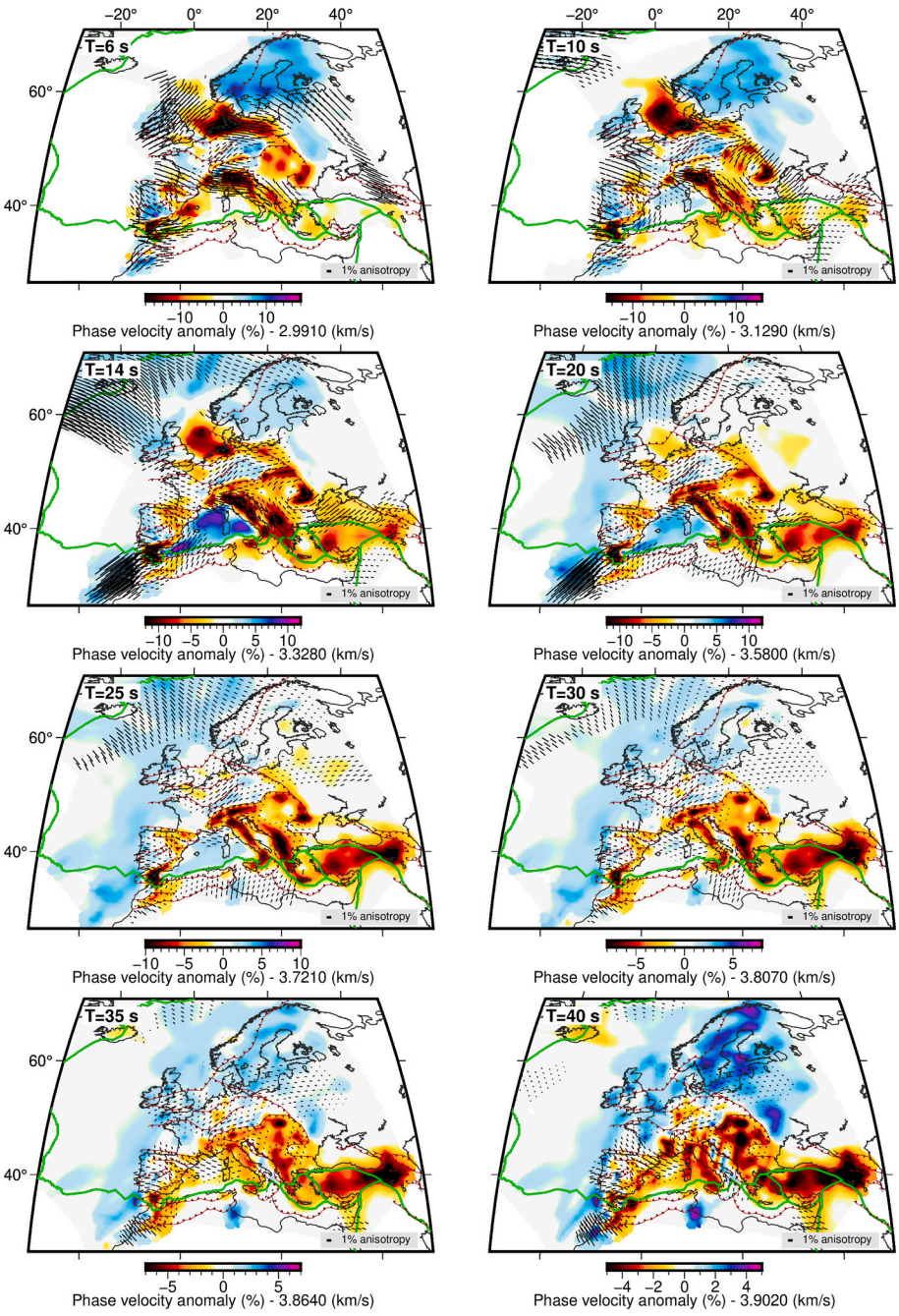

Fig. 12. Azimuthally anisotropic phase-velocity maps for the study region, showing isotropic phase-velocity anomaly and 2ψ anisotropy (same periods as in Fig. 5). In each case, the isotropic phase velocity is plotted relative to the average phase velocity for the given period (labelled on each panel). Anisotropy results are shown only where azimuthal path coverage is sufficient for the results to be robust. Plate boundaries are shown in green. (For interpretation of the references to colour in this figure legend, the reader is referred to the web version of this article.)

orientation. The pattern supports hypotheses invoking a retreating slab in the area (e.g., Bokelmann et al., 2011; Civiero et al., 2020; Díaz et al., 2010). A predominantly NW–*SE*-oriented pattern is well resolved northerly in the Iberian Chain and Meseta and is likely related to the Variscan trend in the area (Díaz et al., 1998).

5.2. *Alpine-Apennines domain*

The Alpine tectonic domain includes an orogenic system formed by the convergence of the Adriatic and European plates. The Adriatic plate is a microplate of oceanic and continental origin and its interaction with the European and African converging plates has given rise to the arcuate Alpine-Mediterranean mountain belt (Dewey et al., 1989; Faccenna and Becker, 2010). The arc reflects multiple episodes of slab retreat since 85 Ma, which occurred in the Alps, Apennines, and Carpathians. These processes have contributed to the complex subduction geometries seen today (e.g., Király et al., 2018). The Adriatic block is the upper plate in the Western-Central Alps and the Western Carpathians but it represents the lower plate in the Apennines and the Dinarides (Handy et al., 2015; Spakman and Wortel, 2004).

Due to their tectonically complex setting, the Alpine and Apennines mountain ranges have been the subject of numerous surface-wave studies (e.g., Boschi et al., 2004; Calcagnile, 1990; El-Sharkawy et al., 2024; Kästle et al., 2018; Magrini et al., 2022; Molinari et al., 2015;

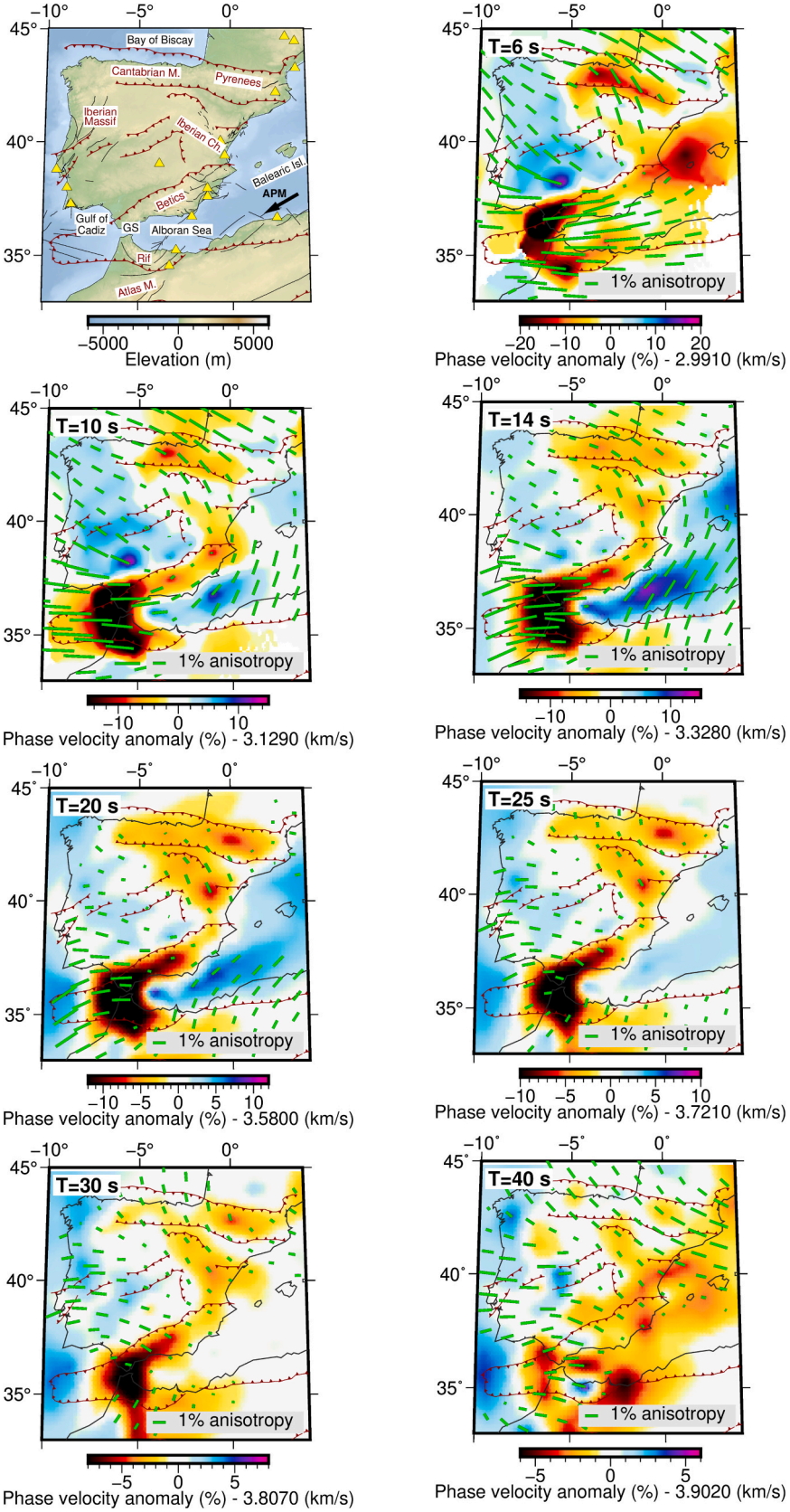

(caption on next page)

Fig. 13. Azimuthally anisotropic maps of Rayleigh-wave phase velocities in the Iberian Peninsula at periods of 6, 10, 14, 20, 25, 30, and 40 s. The first panel shows the topography and the main features discussed in the text. The Cenozoic volcanic fields (Legendre et al., 2012) are indicated with yellow triangles. The crustal faults are taken from the European Fault-Source Model 2020 (EFSM20, https://seismofaults.eu/efsm20). The APM motion in the HS3-Nuvel1A fixed hotspot frame (Gripp and Gordon, 2002) is indicated with a thick black arrow. Green sticks indicate the fast-propagation directions and strength of azimuthal anisotropy 2Ψ. Anisotropy results are shown only where azimuthal path coverage is sufficient for the results to be robust (threshold at 30 %, which means that if the anisotropy bends back to its original position more than 30 %, it does not pass the anisotropy test). GS: Gibraltar Strait. (For interpretation of the references to colour in this figure legend, the reader is referred to the web version of this article.)

Schivardi and Morelli, 2009). Several studies using ambient noise in the Alps and the Apennines agree in mapping similar large-scale isotropic structures (Alder et al., 2021; Fry et al., 2010; Li et al., 2010; Nouibat et al., 2023; Soergel et al., 2023; Stehly et al., 2009; Verbeke et al., 2012). The presence and trend of azimuthal anisotropy in the lithosphere is more debated (e.g., Díaz et al., 2013; Fry et al., 2010; Mele et al., 1998; Pondrelli et al., 2023; Salimbeni et al., 2013; Schmid et al., 2004). Babuska and Plomerová (1992) and Plomerová (1997) identified high-velocity foliation planes E-dipping in the Alpine mantle lithosphere, and high velocities dipping consistently to the SW in the sub-lithosphere below the Apennines. Mele et al. (1998) found that Pn velocity fast directions follow the strike of the Northern Apennines and the Calabrian arcs. The tomography model of Díaz et al. (2013) shows anisotropy parameters with fast directions following the trends of the Alps and Northern Apennines but shifting to NNE–SSW in the Adria region and a large E–W component beneath Tuscany. A regional ambient-noise study reveals that the fast direction of the anisotropy beneath the Central Alps is orogen-parallel above ~30 km but strongly orogen-perpendicular at deeper depths between 30 and 70 km (Fry et al., 2010). They attribute this opposite pattern to the presence of distinct fabrics within the central Alpine lithosphere, each with different geodynamic origins: the orogen-parallel anisotropy is the LPO of crustal minerals, such as amphibole and biotite, resulting from compression while the orogen-perpendicular anisotropy may be attributed to the LPO of olivine, driven by the southward bending and flow of the European lithospheric mantle. It is clear that disagreements over the explanation of anisotropy remain and a conclusive determination of the anisotropic fabric at lithospheric depths can help us to reconstruct the current and past deformation pattern in these orogens.

In the Alps, our anisotropic results at periods <30 s reveal an arc-shaped azimuthal pattern of fast-polarization directions. These range from a dominant WNW–ESE orientation in the Western Alps, to a NE–SW orientation in the Central Alps, and an E–W trend in the Eastern Alps (Fig. 14). At the longest periods, the anisotropy is much weaker and limits tectonic interpretation. In the adjacent Dinarides, the anisotropy aligns with the strike of the range, showing a dominant NW–SE orientation.

Southward, the anisotropy is less well-resolved. Along the Northern Apennine orogen, the fast axes directions are characterized by a pattern with roughly NW–SE orientations. In the Tyrrhenian Basin, the anisotropy is resolved only at periods >25 s showing a moderate E–W fast direction orientation, similar to that retrieved from the tomography model of Díaz et al. (2013). At shorter periods, anisotropy is barely resolved due to the low resolution of the phase-velocity maps (see Fig. 8). This trend can be related to the oblique trench retreat of the Northern Apennines occurring since 5 Ma (Malinverno and Ryan, 1986; Rosenbaum et al., 2002).

Moving towards the Ligurian-Provençal Basin, the anisotropy is higher with an NW–SE trend, likely reflecting the 30° counter-clockwise rotation of the Corsica-Sardinia block from NE Spain in Late Oligocene–Early Miocene (Auzende et al., 1973; Carminati et al., 1998; Maffione et al., 2008). Along the Calabrian Arc, at longer periods ($T > 25$ s) the anisotropy, while weak, exhibits a NE–SW orientation that mirrors the curvature of the arc itself. This implies that a minor influence of the Calabrian slab on the anisotropy exists although the signal is likely dominated by the mantle wedge or the asthenosphere, as suggested by Baccheschi et al. (2011).

Overall, our findings in this region of interest are in line with recent compilations of the present-day crustal tectonic stress (Heidbach et al., 2018) and strain-rate directions (Palano, 2015) in the region.

5.3. North-Central Europe

The lithosphere of North-Central Europe was shaped by a series of continent-continent collisions involving Gondwana-derived microplates during the Caledonian and Variscan orogenic cycles (Matte, 2001; Pharaoh, 1999). These tectonic processes resulted in the closure of several oceanic basins, including the Iapetus, Tornquist, Rheic, and Galicia-Southern Brittany Basins (Winchester et al., 2002). The Avalonia microcontinent rifted off from Gondwana during the Ordovician and made contact with Baltica, thus closing the Iapetus Ocean and producing the Caledonian tectonic belt (Cocks, 2000). The western boundary of this orogenic belt, known as the Caledonian Front, marks the transition between regions affected by Caledonian mountain-building and those that remained geologically unaffected (Ziegler, 1982). One of the most significant lithospheric boundaries in Central Europe is the TTSZ, which cuts through the Polish Trough. This suture separates the tectonically active Phanerozoic lithosphere of Western Europe from the stable Precambrian Eastern European Craton (EEC), marking a major collision zone between these distinct geological domains. Further south, the Mid-German Crystalline Rise represents the Rheic suture, formed by the final closure of the Rheic Ocean during the collision between Avalonia and the micro-terranes of Cadomia/Saxo-Thuringia (Franke, 2000).

Numerous surface-wave studies focused on imaging the crustal and mantle lithosphere structure of North-Central Europe (e.g., Meier et al., 2016; Meier and Malischewsky, 1997; Roux et al., 2011a; Snieder, 1988; Soomro et al., 2016; Yang et al., 2007; Zhu and Tromp, 2013). The phase-velocity maps of Soomro et al. (2016) show in detail the correlation between the low-velocity anomalies at the shortest periods with the thick sedimentary basins of the North German Basin, North Sea Basin, and the Polish Trough as well as the regions of the Cenozoic volcanism. The properties of the lithosphere around the TTSZ are also clearly imaged in all the most recent surface-wave models (El-Sharkawy et al., 2024; Legendre et al., 2012; Soomro et al., 2016). As for the rest of Europe, the regional anisotropic fabric at crustal and lithospheric mantle depths is less explored. A map of the azimuthal anisotropy at 50 km depth in Central Europe is provided by the tomography model of Zhu and Tromp (2013) and shows how some features are well correlated with historical tectonic events in this region, but the shallower-depth anisotropic structure is unknown.

In our phase-velocity maps, the anisotropy in North-Central Europe exhibits a general NE–SW trend, sub-parallel to the strike of the Variscan Front and Rheic Suture at a 10 s period and greater, reflecting the alignment of rock fabric in response to tectonic compression (Fig. 15). This is in line with the results of a joint inversion of magnetotelluric and surface-wave data beneath a small region in Central Germany that indicates the presence of an anisotropic layer with a NE–SW fast-propagation direction at lower-crustal/upper-lithospheric depths (Roux et al., 2011b). Earlier shear-wave splitting and travel-times analyses agree in finding the same layer of the fast direction close to NE–SW in the sub-crustal lithosphere (Babuska and Plomerová, 1992; Bamford, 1977; Vinnik et al., 1994).

At the TTSZ block boundary, a shift in the anisotropy direction is observed. At the shortest periods (< 10 s), the fast directions show a weak NW–SE orientation. At intermediate and longer periods, the anisotropy shifts to a weaker E–W trend. This evidence is in agreement

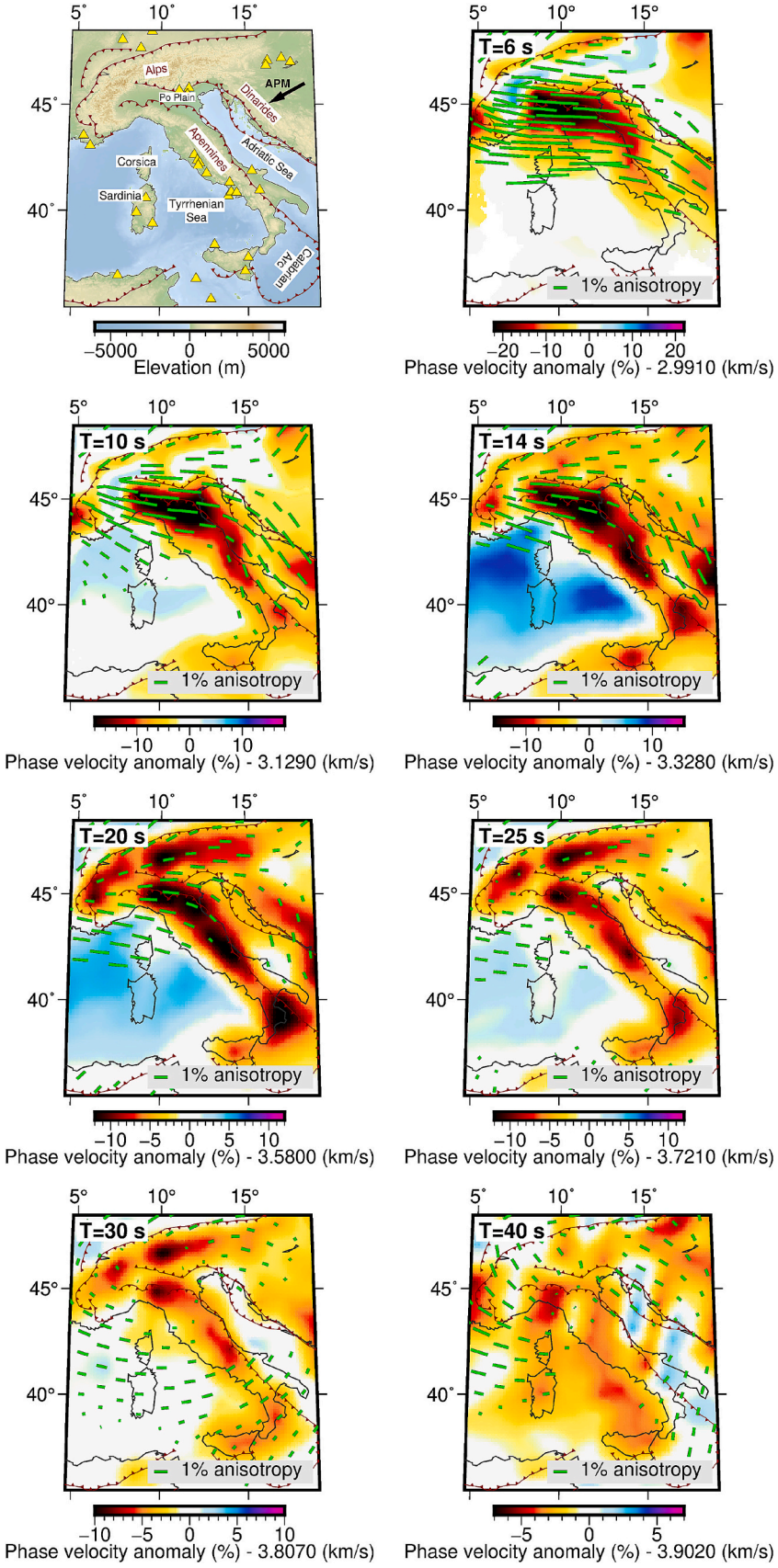

Fig. 14. Same as Fig. 13 for the Alpine-Apennines region. The first panel shows the topography and the main features discussed in the text. The Cenozoic volcanic fields are indicated with yellow triangles. The APM motion in the HS3-Nuvel1A fixed hotspot frame is shown with a thick black arrow. (For interpretation of the references to colour in this figure legend, the reader is referred to the web version of this article.)

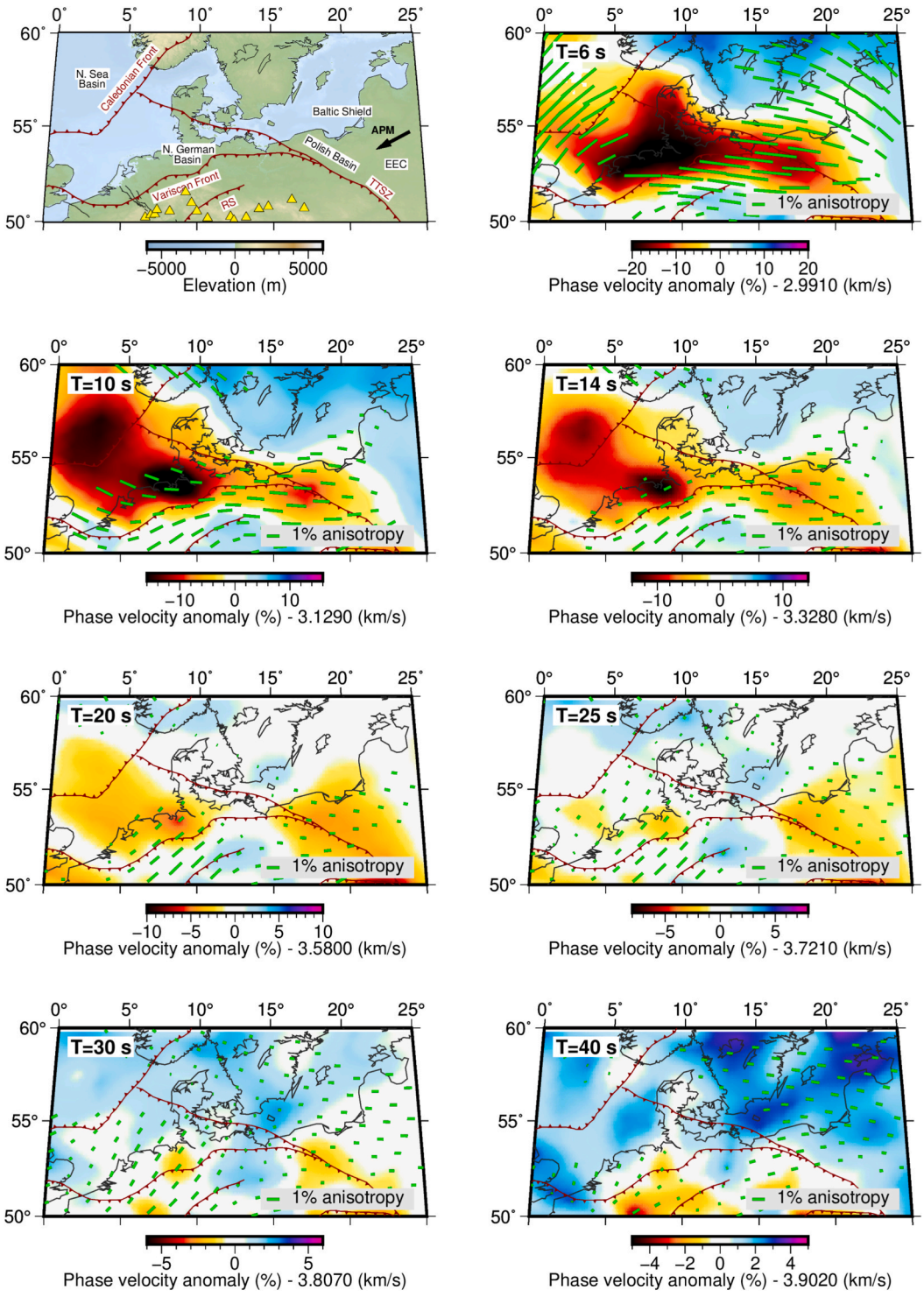

Fig. 15. Same as Fig. 14 for North-Central Europe. The first panel shows the topography and the main features discussed in the text. The Cenozoic volcanic fields are indicated with yellow triangles. The APM motion in the HS3-Nuvel1A fixed hotspot frame is shown with a thick black arrow. TTSZ: Tornquist-Teisseyre Suture Zone; EEC: East European Craton, RS: Rheic Suture. (For interpretation of the references to colour in this figure legend, the reader is referred to the web version of this article.)

with the results of Babuška and Plomerová (2006), which found consistent fossil fabric within different lithospheric blocks created before the assembly of the European landmass.

Overall, the observed anisotropy patterns shed light on both ancient and active tectonic processes, highlighting the complex interplay between past deformation and current stress fields across Europe.

6. Conclusions

To better understand European tectonics and its implications, this study uses sets of two-station Rayleigh wave dispersion curves at periods ranging between 4 and 40 s to tomographically image variations in both seismic velocity and seismic anisotropy in the crust and uppermost mantle beneath the continent.

The lithospheric structure is interpreted in three target regions (the Iberian Peninsula, the Alps-Apennines system, and North-Central Europe) where the data coverage is optimal, and the mapping of anisotropy is unlikely to be biased by either velocity variations or non-comprehensive azimuthal path coverage. The main results are the following:

1) The isotropic shear wave speeds show numerous structures correlated with the geology of the region. The most prominent low-velocity anomalies in the shortest-period maps (<20 s) coincide with the major Cenozoic sedimentary cover. At longer periods, velocity patterns reveal variations in crustal thickness with low-velocity features imaged beneath thickened crust (mountain belts). In some regions of thin lithosphere—where the LAB is shallower than 80 km depth (e.g., Eifel, Massif Central, East Anatolia)—low-velocity anomalies can indicate the presence of mantle upwellings. High velocities have been found under cratonic regions (e.g., EEC, Baltic Shield) indicating a cold, depleted lithosphere.
2) At short periods, crustal-level anisotropy shows fast directions that align with the major mountain ranges of southern Europe (e.g., Betics, Pyrenees, Apennines, Dinarides, Alps), suggesting significant shear deformation in the crust.
3) At longer periods, anisotropy in the shallow lithospheric mantle is weak and exhibits a complex pattern, especially in North-Central Europe. Notably, the Tornquist-Teisseyre suture zone separates the N*E*-oriented anisotropic fabric of the Western European domain (sub-parallel to the Variscan Front) from the E-W trend of the East European cratonic core.

These findings provide new insights into the tectonic evolution and deformation processes shaping the lithosphere of Europe.

CRediT authorship contribution statement

Chiara Civiero: Writing – original draft, Visualization, Software, Project administration, Methodology, Investigation, Funding acquisition, Formal analysis, Conceptualization. **Raffaele Bonadio:** Writing – original draft, Software, Methodology, Investigation, Conceptualization. **Antonio Villaseñor:** Writing – original draft, Software, Methodology, Investigation, Data curation.

Declaration of competing interest

The authors declare that they have no known competing financial interests or personal relationships that could have appeared to influence the work reported in this paper.

Acknowledgments

The authors thank the Editor and two anonymous reviewers for valuable suggestions. We are grateful to the operators of seismic networks and arrays who have created and made available the broadband seismic data that was used in the original measurements. We thank all the data centers for providing the waveform data used. This work acknowledges the 'Severo Ochoa Centre of Excellence' accreditation CEX2019-000928-S funded by AEI 10.13039/501100011033 and it has been completed in the framework of the Program for Young Researchers "Rita Levi Montalcini" (grant D86-RALMI23CIVIE_01 awarded by the Italian Ministry of University and Research). CC and RB were supported by the Science Foundation Ireland (SFI) grant 16/IA/4598, co-funded by the Geological Survey of Ireland and the Marine Institute, UK Natural Environment Research Council (grant NE/X000060/1), Project InnerSpace (https://projectinnerspace.org/) and the project 4D Dynamic Earth, funded by ESA (4000140327/23/NL/SD) as part of EXPRO+. We thank Sergei Lebedev for the helpful discussions and for providing the code for inversion. All the maps were generated using Generic Mapping Tools (GMT) (Wessel et al., 2013).

Appendix A. Supplementary data

Supplementary data to this article can be found online at https://doi.org/10.1016/j.tecto.2025.230788.

Data availability

Data will be made available on request.

References

Acevedo, J., Fernández-Viejo, G., Llana-Fúnez, S., López-Fernández, C., 2020. Upper-Crustal Seismic Anisotropy in the Cantabrian Mountains (North Spain) from Shear-Wave Splitting and Ambient Noise Interferometry Analysis. Seismol. Res. Lett. https://doi.org/10.1785/0220200103.

Alder, C., Debayle, E., Bodin, T., Paul, A., Stehly, L., Pedersen, H., 2021. Evidence for radial anisotropy in the lower crust of the Apennines from Bayesian ambient noise tomography in Europe. Geophys. J. Int. 941–967. https://doi.org/10.1093/gji/ggab066.

Alpert, L.A., Miller, M.S., Becker, T.W., Allam, A.A., 2013. Structure beneath the Alboran from geodynamic flow models and seismic anisotropy. J. Geophys. Res. Solid Earth 118, 4265–4277. https://doi.org/10.1002/jgrb.50309.

Arroucau, P., Cust, S., Civiero, C., Silveira, G., Dias, N., Villase, A., Bodin, T., 2021. PRISM3D: a 3-D reference seismic model for Iberia and adjacent areas. Geophys. J. Int. 789–810. https://doi.org/10.1093/gji/ggab005.

Auzende, J.M., Bonnin, J., Olivet, J.L., 1973. The origin of the western Mediterranean basin. J. Geol. Soc. Lond. 129, 607–620. https://doi.org/10.1144/gsjgs.129.6.0607.

Babuska, V., Cara, M., 1991. Seismic Anisotropy in the Earth. Springer Science & Business Media.

Babuska, V., Plomerová, J., 1992. The lithosphere in Central Europe-seismological and petrological aspects. Tectonophysics 207, 141–163.

Babuška, V., Plomerová, J., 2006. European mantle lithosphere assembled from rigid microplates with inherited seismic anisotropy. Phys. Earth Planet. Inter. 158, 264–280. https://doi.org/10.1016/j.pepi.2006.01.010.

Baccheschi, P., Margheriti, L., Steckler, M.S., Boschi, E., 2011. Anisotropy patterns in the subducting lithosphere and in the mantle wedge: a case study—the southern Italy subduction system. J. Geophys. Res. 116, B08306. https://doi.org/10.1029/2010JB007961.

Bamford, D., 1977. Pn velocity anisotropy in a continental upper mantle. Geophys. J. R. Astron. Soc. 49, 29–48.

Bao, X., Song, X., Eaton, D.W., Xu, Y., Chen, H., 2020. Episodic Lithospheric Deformation in Eastern Tibet Inferred from Seismic Anisotropy. Geophys. Res. Lett. 47. https://doi.org/10.1029/2019GL085721 e2019GL085721.

Barruol, G., Mainprice, D., 1993. A quantitative evaluation of the contribution of crustal rocks to the shear-wave splitting of teleseismic SKS waves. Phys. Earth Planet. Inter. 78, 281–300. https://doi.org/10.1016/0031-9201(93)90161-2.

Becker, T.W., Lebedev, S., Long, M.D., 2012. On the relationship between azimuthal anisotropy from shear wave splitting and surface wave tomography. J. Geophys. Res. Solid Earth 117, 1–17. https://doi.org/10.1029/2011JB008705.

Bensen, G.D., Ritzwoller, M.H., Barmin, M.P., Levshin, A.L., Lin, F., Moschetti, M.P., Shapiro, N.M., Yang, Y., 2007. Processing seismic ambient noise data to obtain reliable broad-band surface wave dispersion measurements. Geophys. J. Int. 1239–1260. https://doi.org/10.1111/j.1365-246X.2007.03374.x.

Bensen, G.D., Ritzwoller, M.H., Shapiro, N.M., 2008. Broadband ambient noise surface wave tomography across the United States. J. Geophys. Res. 113. https://doi.org/10.1029/2007JB005248, 2007JB005248.

Bensen, G.D., Ritzwoller, M.H., Yang, Y., 2009. A 3-D shear velocity model of the crust and uppermost mantle beneath the United States from ambient seismic noise. Geophys. J. Int. 177, 1177–1196. https://doi.org/10.1111/j.1365-246X.2009.04125.x.

Bokelmann, G., Maufroy, E., Buontempo, L., Morales, J., Barruol, G., 2011. Testing oceanic subduction and convective removal models for the Gibraltar arc: Seismological constraints from dispersion and anisotropy. Tectonophysics 502, 28–37. https://doi.org/10.1016/j.tecto.2010.08.004.

Bonadio, R., Lebedev, S., Meier, T., Arroucau, P., Schaeffer, A.J., Licciardi, A., Agius, M. R., Horan, C., Collins, L., O'Reilly, B.M., Readman, P.W., 2021. Optimal resolution tomography with error tracking and the structure of the crust and upper mantle beneath Ireland and Britain. Geophys. J. Int. 226, 2158–2188. https://doi.org/10.1093/gji/ggab169.

Boschi, L., Ekström, G., Kustowski, B., 2004. Multiple resolution surface wave tomography: the Mediterranean basin. Geophys. J. Int. 157, 293–304. https://doi.org/10.1111/j.1365-246X.2004.02194.x.

Calcagnile, G., Panza, 1990. Crustal and upper mantle structure of the Mediterranean area derived derived from Surface-Wave Data. Phys. Earth Planet. Inter. 60, 163–168.

Carminati, E., Wortel, M.J.R., Spakman, W., Sabadini, R., 1998. The role of slab detachment processes in the opening of the western – Central Mediterranean basins: some geological and geophysical evidence. Earth Planet. Sci. Lett. 160, 651–665.

Celli, N.L., Lebedev, S., Schaeffer, A.J., Gaina, C., 2021. The tilted Iceland Plume and its effect on the North Atlantic evolution and magmatism. Earth Planet. Sci. Lett. 569, 117048. https://doi.org/10.1016/j.epsl.2021.117048.
Chevrot, S., Villasenor, A., Sylvander, M., Benahmed, S., Beucler, E., Cougoulat, G., Delmas, P., Blanquat, M.D.S., Diaz, J., Gallart, J., Grimaud, F., Lagabrielle, Y., Manatschal, G., Mocquet, A., Pauchet, H., Paul, A., Péquegnat, C., Quillard, O., Roussel, S., Ruiz, M., Wolyniec, D., 2014. High-resolution imaging of the Pyrenees and Massif Central from the data of the PYROPE and IBERARRAY portable array deployments. J. Geophys. Res. Solid Earth 119, 6399–6420. https://doi.org/10.1002/2014JB010953.
Cho, K.H., Herrmann, R.B., Ammon, C.J., Lee, K., 2007. Imaging the upper crust of the Korean peninsula by surface-wave tomography. Bull. Seismol. Soc. Am. 97, 198–207. https://doi.org/10.1785/0120060096.
Chourak, M., Corchete, V., Badal, J., Gómez, F., Serón, J., 2005. Shallow seismic velocity structure of the Betic cordillera (Southern Spain) from modelling of Rayleigh wave dispersion. Surv. Geophys. 26, 481–504. https://doi.org/10.1007/s10712-005-7260-4.
Christensen, N.I., 1984. The magnitude, symmetry and origin of upper mantle anisotropy based on fabric analyses of ultramafic tectonites. Geophys. J. Int. 76 (1), 89–111.
Civiero, C., Custódio, S., Duarte, J.C., Mendes, V.B., Faccenna, C., 2020. Dynamics of the Gibraltar Arc System: a complex Interaction between Plate Convergence, Slab pull, and Mantle Flow. J. Geophys. Res. Solid Earth 125, 1–23. https://doi.org/10.1029/2019JB018873.
Civiero, C., Lebedev, S., Celli, N.L., 2022. A complex mantle plume head below east africa-arabia shaped by the lithosphere-asthenosphere boundary topography. Geochem. Geophys. Geosyst. https://doi.org/10.1029/2022GC010610.
Civiero, C., Celli, N.L., Tesauro, M., 2023. Revisiting the geodynamics of the Middle East region from an integrated geophysical perspective. J. Geodyn. 158, 102005. https://doi.org/10.1016/j.jog.2023.102005.
Cocks, L.R.M., 2000. The early Palaeozoic geography of Europe. J. Geol. Soc. Lond. 157, 1–10. https://doi.org/10.1144/jgs.157.1.1.
Corchete, V., Chourak, M., 2011. Shear-wave velocity structure of the south-eastern part of the Iberian Peninsula from Rayleigh wave analysis. Int. J. Earth Sci. 100, 1733–1747. https://doi.org/10.1007/s00531-010-0581-7.
Corchete, V., Badal, J., Serón, F.J., Soria, A., 1995. Tomographic images of the Iberian subcrustal lithosphere and asthenosphere. J. Geophys. Res. 100, 24133–24146. https://doi.org/10.1029/95JB00979.
Crampin, S., 1984. Effective anisotropic elastic constants for wave propagation through cracked solids. Geophys. J. R. Astron. Soc. 76, 135–145.
Crampin, S., Peacock, S., 2008. A review of the current understanding of seismic shear-wave splitting in the Earth's crust and common fallacies in interpretation. Wave Motion 45, 675–722.
Custódio, S., Dias, N.A., Caldeira, B., Carrilho, F., Carvalho, S., Corela, C., Díaz, J., Narciso, J., Madureira, G., Matias, L., Haberland, C., 2014. Ambient noise recorded by a dense broadband seismic deployment in Western Iberia. Bull. Seismol. Soc. Am. 104, 2985–3007. https://doi.org/10.1785/0120140079.
Darbyshire, F.A., Lebedev, S., 2009. Rayleigh wave phase-velocity heterogeneity and multilayered azimuthal anisotropy of the Superior Craton, Ontario. Geophys. J. Int. 176, 215–234. https://doi.org/10.1111/j.1365-246X.2008.03982.x.
Dewey, J.F., Helman, M.L., Turco, E., Hutton, D.H.W., Knott, S.D., 1989. Kinematics of the western Mediterranean. Geol. Soc. Lond. Spec. Publ. 265–283.
Díaz, J., Gallart, J., Hirn, A., Paulssen, H., 1998. Anisotropy beneath the Iberian Peninsula: the contribution of the ILIHA-NARS broad-band experiment. Pure Appl. Geophys. 151, 395–405. https://doi.org/10.1007/s000240050119.
Díaz, J., Villaseñor, A., Gallart, J., Morales, J., Pazos, A., Córdoba, D., Pulgar, J.A., García-Lobón, J.L., Harnafi, M., TopoIberia Seismic Working Group, 2009. The IBERARRAY broadband seismic network: a new tool to investigate the deep structure beneath Iberia. Orfeus Newsl. 8, 1–6.
Díaz, J., Gallart, J., Villaseñor, A., Mancilla, F., Pazos, A., Córdoba, D., Pulgar, J.A., Ibarra, P., Harnafi, M., 2010. Mantle dynamics beneath the Gibraltar Arc (western Mediterranean) from shear-wave splitting measurements on a dense seismic array. Geophys. Res. Lett. 37, 1–5. https://doi.org/10.1029/2010GL044201.
Díaz, J., Gil, A., Gallart, J., 2013. Uppermost mantle seismic velocity and anisotropy in the Euro-Mediterranean region from Pn and Sn tomography. Geophys. J. Int. 192, 310–325. https://doi.org/10.1093/gji/ggs016.
Dziewonski, A.M., Anderson, D.L., 1981. Preliminary reference Earth model. Phys. Earth Planet. Inter. 25, 297–356. https://doi.org/10.1016/0031-9201(81)90046-7.
Ekström, G., 2011. A global model of love and Rayleigh surface wave dispersion and anisotropy, 25-250s. Geophys. J. Int. 187, 1668–1686. https://doi.org/10.1111/j.1365-246X.2011.05225.x.
El-Sharkawy, A., Meier, T., Lebedev, S., Behrmann, J., Hamada, M., Cristiano, L., Weidle, C., Köhn, D., 2020. The Slab Puzzle of the Alpine-Mediterranean Region: Insights from a New. Geochemistry, Geophysics, Geosystems, High-Resolution, Shear-Wave Velocity Model of the Upper Mantle. https://doi.org/10.1029/2020GC008993.
El-Sharkawy, A., Hansteen, T.H., Clemente-Gomez, C., Fullea, J., Lebedev, S., Meier, T., 2024. Cenozoic Volcanic Provinces and Shallow Asthenospheric Volumes in the Circum-Mediterranean: evidence from Magmatic Geochemistry, Seismic Tomography, and Integrated Geophysical-Petrological Thermochemical Inversion. Geochem. Geophys. Geosyst. 25. https://doi.org/10.1029/2023GC011017 e2023GC011017.
Faccenna, C., Becker, T.W., 2010. Shaping mobile belts by small-scale convection. Nature 465, 602–605. https://doi.org/10.1038/nature09064.
Feng, L., Díaz, J., 2022. Azimuthal anisotropy of the westernmost Mediterranean : New constraints on lithospheric deformation and geodynamical evolution. Earth Planet. Sci. Lett. 593, 117689. https://doi.org/10.1016/j.epsl.2022.117689.
Feng, L., Diaz, J., 2023. A High-Resolution Shear Velocity Model of the Crust and Uppermost Mantle beneath Westernmost Mediterranean Including Radial Anisotropy. Journal of Geophysical Research: Solid. Earth 128. https://doi.org/10.1029/2023JB026868 e2023JB026868.
Franke, W., 2000. The mid-European segment of the Variscides: tectonostratigraphic units, terrane boundaries and plate tectonic evolution. Geol. Soc. Lond. Spec. Publ. 179, 35–61. https://doi.org/10.1144/GSL.SP.2000.179.01.05.
Fry, B., Deschamps, F., Kissling, E., Stehly, L., Giardini, D., 2010. Layered azimuthal anisotropy of Rayleigh wave phase velocities in the European Alpine lithosphere inferred from ambient noise. Earth Planet. Sci. Lett. 297, 95–102. https://doi.org/10.1016/j.epsl.2010.06.008.
Fullea, J., Lebedev, S., Martinec, Z., Celli, N.L., 2021. WINTERC-grav: mapping the upper mantle thermochemical heterogeneity from coupled geophysical-petrological inversion of seismic waveforms, heat flow, surface elevation and gravity satellite data. Geophys. J. Int. 226, 146–191. https://doi.org/10.1093/gji/ggab094.
Gibbons, W., Moreno, T., 2002. The Geology of Spain. Geol. Soc., London 650.
Goes, S., Spakman, W., Bijwaard, H., 1999. A lower mantle source for central European volcanism. Science 286, 1928–1934. https://doi.org/10.1126/science.286.5446.1928.
Gripp, A.E., Gordon, R.G., 2002. Young tracks of hotspots and current plate velocities. Geophys. J. Int. 150, 321–361. https://doi.org/10.1046/j.1365-246X.2002.01627.x.
Handy, M.R., Ustaszewski, K., Kissling, E., 2015. Reconstructing the Alps – Carpathians – Dinarides as a key to understanding switches in subduction polarity, slab gaps and surface motion. Int. J. Earth Sci. 1–26. https://doi.org/10.1007/s00531-014-1060-3.
Heidbach, O., Rajabi, M., Cui, X., Fuchs, K., Müller, B., Reinecker, J., Reiter, K., Tingay, M., Wenzel, F., Xie, F., Ziegler, M.O., Zoback, M.L., Zoback, M., 2018. The World stress Map database release 2016: Crustal stress pattern across scales. Tectonophysics 744, 484–498. https://doi.org/10.1016/j.tecto.2018.07.007.
Kästle, E.D., El-Sharkawy, A., Boschi, L., Meier, T., Rosenberg, C., Bellahsen, N., Cristiano, L., Weidle, C., 2018. Surface Wave Tomography of the Alps using Ambient-Noise and earthquake phase Velocity Measurements. J. Geophys. Res. Solid Earth 123, 1770–1792. https://doi.org/10.1002/2017JB014698.
Kennett, B.L.N., Engdahl, E.R., Buland, R., 1995. Constraints on seismic velocities in the Earth from travel times. Geophys. J. Int. 122, 108–124. https://doi.org/10.1111/j.1365-246X.1995.tb03540.x.
Király, Á., Faccenna, C., Funiciello, F., 2018. Subduction zones Interaction around the Adria Microplate and the Origin of the Apenninic Arc. Tectonics 37, 3941–3953. https://doi.org/10.1029/2018TC005211.
Laske, G., Masters, G., Ma, Z., Pasyanos, M.E., 2013. CRUST1.0: an Updated Global Model of Earth's CRUST. Geophys. Res. Abstr. 15. Abstract EGU2013–2658.
Le Pichon, X., Chamot-rooke, N., Noomen, R., 1995. Geodetic determination of the kinematics of Central Greece with respect to Europe : Implications for eastern Mediterranean tectonics. J. Geophys. Res. 100, 675–690. https://doi.org/10.1029/95JB00317.
Lebedev, S., Van Der Hilst, R.D., 2008. Global upper-mantle tomography with the automated multimode inversion of surface and S-wave forms. Geophys. J. Int. 173, 505–518. https://doi.org/10.1111/j.1365-246X.2008.03721.x.
Legendre, C.P., Meier, T., Lebedev, S., Friederich, W., Viereck-Götte, L., 2012. A shear wave velocity model of the European upper mantle from automated inversion of seismic shear and surface waveforms. Geophys. J. Int. 191, 282–304. https://doi.org/10.1111/j.1365-246X.2012.05613.x.
Li, H., Bernardi, F., Michelini, A., 2010. Surface wave dispersion measurements from ambient seismic noise analysis in Italy. Geophys. J. Int. 180, 1242–1252. https://doi.org/10.1111/j.1365-246X.2009.04476.x.
Lin, F.C., Moschetti, M.P., Ritzwoller, M.H., 2008. Surface wave tomography of the western United States from ambient seismic noise: Rayleigh and love wave phase velocity maps. Geophys. J. Int. 173, 281–298. https://doi.org/10.1111/j.1365-246X.2008.03720.x.
Lin, F.C., Li, D., Clayton, R.W., Hollis, D., 2013. High-resolution 3D shallow crustal structure in Long Beach, California: Application of ambient noise tomography on a dense seismic array. Geophysics 78. https://doi.org/10.1190/geo2012-0453.1.
Link, F., Rümpker, G., 2023. Shear-Wave Splitting reveals Layered-Anisotropy beneath the European Alps in Response to Mediterranean Subduction. Journal of Geophysical Research: Solid. Earth 128. https://doi.org/10.1029/2023JB027192 e2023JB027192.
Lloyd, G.E., Butler, R.W.H., Casey, M., Mainprice, D., 2009. Mica, deformation fabrics and the seismic properties of the continental crust. Earth Planet. Sci. Lett. 288, 320–328. https://doi.org/10.1016/j.epsl.2009.09.035.
Long, M.D., Silver, P.G., 2008. The Subduction Zone Flow Field from Seismic Anisotropy: a Global View. Science 319, 315–319.
Lu, Y., Stehly, L., Paul, A., 2018. High-resolution surface wave tomography of the European crust and uppermost mantle from ambient seismic noise. Geophys. J. Int. 214, 1136–1150. https://doi.org/10.1093/gji/ggy188.
Macquet, M., Paul, A., Pedersen, H.A., Villaseñor, A., Chevrot, S., Sylvander, M., Wolyniec, D., 2014. Ambient noise tomography of the Pyrenees and the surrounding regions: Inversion for a 3-D Vs model in the presence of a very heterogeneous crust. Geophys. J. Int. 199, 402–415. https://doi.org/10.1093/gji/ggu270.
Maffione, M., Speranza, F., Faccenna, C., Cascella, A., Vignaroli, G., Sagnotti, L., 2008. A synchronous Alpine and Corsica-Sardinia rotation. Journal of Geophysical Research: Solid. Earth 113. https://doi.org/10.1029/2007JB005214, 2007JB005214.
Magrini, F., Diaferia, G., El-Sharkawy, A., Cammarano, F., van der Meijde, M., Meier, T., Boschi, L., 2022. Surface-Wave Tomography of the Central-Western Mediterranean: New Insights into the Liguro-Provençal and Tyrrhenian Basins. J. Geophys. Res. Solid Earth 127. https://doi.org/10.1029/2021JB023267.

Mainprice, D., Barruol, G., Isma, W.B., 2010. The Seismic anisotropy of the Earth ' s mantle: from single crystal to polycrystal. Geophys. Monograph Series. 237–264.
Malcolm, A.E., Scales, J.A., Van Tiggelen, B.A., 2004. Extracting the Green function from diffuse, equipartitioned waves. Phys. Rev. E 70, 015601. https://doi.org/10.1103/PhysRevE.70.015601.
Malinverno, A., Ryan, W.B.F., 1986. Extension in the Tyrrhenian Sea and shortening in the Apennines as result of arc migration driven by sinking of the lithosphere. Tectonics 5, 227–245. https://doi.org/10.1029/TC005i002p00227.
Malory, A.O., Bao, X., Chen, Z., 2022. Crustal shear wave velocity and radial anisotropy beneath Southern Africa from ambient noise tomography. Tectonophysics 822, 229191. https://doi.org/10.1016/j.tecto.2021.229191.
Marone, F., van der Lee, S., Giardini, D., 2004. Shallow anisotropy in the Mediterranean mantle from surface waves. Geophys. Res. Lett. 31, 2–5. https://doi.org/10.1029/2003GL018948.
Matte, P., 2001. The Variscan collage and orogeny (480 ± 290 Ma) and the tectonic definition of the Armorica microplate: a review. Terra Nova 13, 122–128. https://doi.org/10.1046/j.1365-3121.2001.00327.x.
McNamara, D.E., Owens, T.J., 1993. Azimuthal Shear Wave Velocity Anisotropy in the Basin and Range Province using Moho Ps Converted Phases. J. Geophys. Res. 98, 3–12.
Meier, T., Malischewsky, P.G., 1997. Reflection and transmission of surface waves at a vertical discontinuity and imaging of lateral heterogeneity using reflected fundamental Rayleigh waves. Bull. Seismol. Soc. Am. 87, 1648–1661.
Meier, T., Dietrich, K., Stöckhert, B., Harjes, H.P., 2004. One-dimensional models of shear wave velocity for the eastern Mediterranean obtained from the inversion of Rayleigh wave phase velocities and tectonic implications. Geophys. J. Int. 156, 45–58. https://doi.org/10.1111/j.1365-246X.2004.02121.x.
Meier, T., Soomro, R.A., Viereck, L., Lebedev, S., Behrmann, J.H., Weidle, C., Cristiano, L., Hanemann, R., 2016. Mesozoic and Cenozoic evolution of the central European lithosphere. Tectonophysics 692, 58–73. https://doi.org/10.1016/j.tecto.2016.09.016.
Mele, G., Rovelli, A., Seber, D., Hearn, T.M., Barazangi, M., 1998. Compressional velocity structure and anisotropy in the uppermost mantle beneath Italy and surrounding regions Giuliana and. J. Geophys. Res,-Solid Earth 103, 12529–12543. https://doi.org/10.1029/98JB00596.
Michon, L., Van Balen, R.T., Merle, O., Pagnier, H., 2003. The Cenozoic evolution of the Roer Valley Rift System integrated at a European scale. Tectonophysics 367, 101–126. https://doi.org/10.1016/S0040-1951(03)00132-X.
Molinari, I., Verbeke, J., Boschi, L., Kissling, E., Morelli, A., 2015. Italian and Alpine three-dimensional crustal structure imaged by ambient-noise surface-wave dispersion. Geochem. Geophys. Geosyst. 18, 1541–1576. https://doi.org/10.1002/2015GC005746.
Montagner, J.-P., Nataf, H., 1986. A simple method for inverting the azimuthal anisotropy of surface waves. J. Geophys. Res. 91, 511–520. https://doi.org/10.1029/JB091iB01p00511.
Müller, R.D., Sdrolias, M., Gaina, C., Roest, W.R., 2008. Age, spreading rates, and spreading asymmetry of the world's ocean crust. Geochem. Geophys. Geosystems 9, 1–19. https://doi.org/10.1029/2007GC001743.
Nita, B., Maurya, S., Montagner, J.-P., 2016. Anisotropic tomography of the European lithospheric structure from surface wave studies. Geochem. Geophys. Geosyst. 17, 2015–2033. https://doi.org/10.1002/2015GC006243.
Nouibat, A., Brossier, R., Stehly, L., Cao, J., Paul, A., Cifalps Team and AlpArray Working Group, 2023. Ambient-Noise Wave-Equation Tomography of the Alps and Ligurian-Provence Basin. J. Geophys. Res. Solid Earth 128. https://doi.org/10.1029/2023JB026776 e2023JB026776.
Paige, C.C., Saunders, M.A., 1982. Algorithm 583: LSQR: Sparse Linear Equations and Least Squares Problems. ACM Trans. Math. Softw. 8, 195–209. https://doi.org/10.1145/355993.356000.
Palano, M., 2015. On the present-day crustal stress, strain-rate fields and mantle anisotropy pattern of Italy Mimmo. Geophys. J. Int. 200, 967–983. https://doi.org/10.1093/gji/ggu451.
Palomeras Thurner, S., Levander, A., Liu, K., Villaseñor, A., Carbonell, R., Harnafi, M., 2014. Finite-frequency Rayleigh wave tomography of the western Mediterranean: Mapping its lithospheric structure. Geochem. Geophys. Geosyst. 15, 140–160. https://doi.org/10.1002/2013GC004861.
Palomeras, I., Villaseñor, A., Thurner, S., Levander, A., Gallart, J., Harnafi, M., 2017. Lithospheric structure of Iberia and Morocco using finite-frequency Rayleigh wave tomography from earthquakes and seismic ambient noise. Geochem. Geophys. Geosys. Geosys. 1824–1840. https://doi.org/10.1002/2016GC006657.
Panza, G.F., Mueller, St, G, C., 1980. The Gross Features of the Lithosphere-Asthenosphere System in Europe from Seismic Surface Waves and Body Waves. Pure Appl. Geophys. 118, 1209–1213.
Paulssen, H., Levshin, A.L., Lander, A.V., Snieder, R., 1990. Time- and frequency-dependent polarization analysis: anomalous surface wave observations in Iberia. Geophys. J. Int. 103, 483–496. https://doi.org/10.1111/j.1365-246X.1990.tb01786.x.
Pedreira, D., Pulgar, J.A., Gallart, J., Díaz, J., 2003. Seismic evidence of Alpine crustal thickening and wedging from the western Pyrenees to the Cantabrian Mountains (North Iberia). J. Geophys. Res. Solid Earth 108, 1–21. https://doi.org/10.1029/2001jb001667.
Pharaoh, T.C., 1999. Palaeozoic terranes and their lithospheric boundaries within the Trans-European Suture Zone (TESZ): a review. Tectonophysics 314, 17–41. https://doi.org/10.1016/S0040-1951(99)00235-8.
Platt, J.P., Becker, T.W., Evans, R.L., Humpreys, C.T., Lee, C.T.A., Levander, A., 2008. PICASSO: testing models for upper mantle processes beneath the Alboran Basins and the Gibraltar Arc (Western Mediterranean). Geol. Soc. Am. Abstr. Programs 40 (6), 273.
Plomerová, J., 1997. Sesimic anisotropy in tomographic studies of the upper mantle beneath Southern Europe. Ann. Geofis. XL.
Polat, G., Lebedev, S., Readman, P.W., O'Reilly, B.M., Hauser, F., 2012. Anisotropic rayleigh-wave tomography of Ireland's crust: Implications for crustal accretion and evolution within the caledonian orogen. Geophys. Res. Lett. 39. https://doi.org/10.1029/2012GL051014.
Pondrelli, S., Salimbeni, S., Baccheschi, P., Confal, J.M., Margheriti, L., 2023. Peeking inside the mantle structure beneath the Italian region through SKS shear wave splitting anisotropy: a review. Ann. Geophys. 66. https://doi.org/10.4401/ag-8872.
Ribe, N.M., 1989. Seismic anisotropy and mantle flow. J. Geophys. Res. 94, 4213–4223. https://doi.org/10.1029/JB094iB04p04213.
Ribe, N.M., 1992. On the relation between seismic anisotropy and finite strain. J. Geophys. Res. Solid Earth 97, 8737–8747. https://doi.org/10.1029/92JB00551.
Ritzwoller, M.H., Levshin, A.L., 1998. Eurasian surface wave tomography : Group velocities. J. Geophys. Res. Solid Earth 103, 4839–4878. https://doi.org/10.1029/97JB02622.
Rosenbaum, G., Lister, G.S., Duboz, C., 2002. Reconstruction of the tectonic evolution of the western Mediterranean since the Oligocene. J. Virtual Explor. 8, 107–130. https://doi.org/10.3809/jvirtex.2002.00053.
Roux, E., Moorkamp, M., Jones, A.G., Bischoff, M., Endrun, B., Lebedev, S., Meier, T., 2011a. Joint inversion of long-period magnetotelluric data and surface-wave dispersion curves for anisotropic structure: Application to data from Central Germany. Geophys. Res. Lett. 38. https://doi.org/10.1029/2010GL046358.
Roux, E., Moorkamp, M., Jones, A.G., Bischoff, M., Endrun, B., Lebedev, S., Meier, T., 2011b. Joint inversion of long-period magnetotelluric data and surface-wave dispersion curves for anisotropic structure: Application to data from Central Germany. Geophys. Res. Lett. 38. https://doi.org/10.1029/2010GL046358.
Salimbeni, S., Pondrelli, S., Margheriti, L., 2013. Hints on the deformation penetration induced by subductions and collision processes: Seismic anisotropy beneath the Adria region (Central Mediterranean). J. Geophys. Res. Solid Earth 118, 5814–5826. https://doi.org/10.1002/2013JB010253.
Schivardi, R., Morelli, A., 2009. Surface wave tomography in the European and Mediterranean region. Geophys. J. Int. 177, 1050–1066. https://doi.org/10.1111/j.1365-246X.2009.04100.x.
Schmid, C., van der Lee, S., Giardini, D., 2004. Delay times and shear wave splitting in the Mediterranean region. Geophys. J. Int. 159, 275–290. https://doi.org/10.1111/j.1365-246X.2004.02381.x.
Shapiro, N.M., Campillo, M., 2004. Emergence of broadband Rayleigh waves from correlations of the ambient seismic noise. Geophys. Res. Lett. 31. https://doi.org/10.1029/2004GL019491, 2004GL019491.
Shapiro, N.M., Campillo, M., Stehly, L., Ritzwoller, M.H., 2005. High-resolution surface-wave tomography from ambient seismic noise. Science 307, 1615–1618. https://doi.org/10.1126/science.1108339.
Silveira, G., Afonso Dias, N., Villaseñor, A., 2013. Seismic imaging of the western Iberian crust using ambient noise: Boundaries and internal structure of the Iberian Massif. Tectonophysics 589, 186–194. https://doi.org/10.1016/j.tecto.2012.12.025.
Silveira, G., Dias, N.A., Kiselev, S., Stutzmann, E., Custódio, S., Schimmel, M., 2022. Imaging the crust and uppermost mantle structure of Portugal (West Iberia) with seismic ambient noise. Geophys. J. Int. 230, 1106–1120. https://doi.org/10.1093/gji/ggac106.
Snieder, R., 1988. Large-Scale Waveform Inversions of Surface Waves for Lateral Heterogeneity 2. Application to Surface Waves in Europe and the Mediterranean. J. Geophys. Res. 93, 12067–12080. https://doi.org/10.1029/JB093iB10p12067.
Snieder, R., 2004. Extracting the Green's function from the correlation of coda waves: a derivation based on stationary phase. Phys. Rev. E Stat. Phys. Plasmas Fluids Relat. Interdiscip. Topics 69, 8. https://doi.org/10.1103/PhysRevE.69.046610.
Soergel, D., Pedersen, H.A., Bodin, T., Paul, A., Stehly, L., Group, A.W, 2023. Bayesian analysis of azimuthal anisotropy in the Alpine lithosphere from beamforming of ambient noise cross-correlations. Geophys. J. Int. 232, 429–450. https://doi.org/10.1093/gji/ggac349.
Soomro, R.A., Weidle, C., Cristiano, L., Lebedev, S., Meier, T., Wilde-Piórko, M., Geissler, W., Plomerová, J., Grad, M., Babuška, V., Brückl, E., Čyžiene, J., Czuba, W., England, R., Gaczyński, E., Gazdova, R., Gregersen, S., Guterch, A., Hanka, W., Hegedus, E., Heuer, B., Jedlička, P., Lazauskiene, J., Randy Keller, G., Kind, R., Klinge, K., Kolinsky, P., Komminaho, K., Kozlovskaya, E., Krüger, F., Larsen, T., Majdański, M., Málek, J., Motuza, G., Novotný, O., Pietrasiak, R., Plenefisch, T., Råužek, B., Sliaupa, S., Środa, P., Świeczak, M., Tiira, T., Voss, P., Wiejacz, P., 2016. Phase velocities of Rayleigh and love waves in central and northern Europe from automated, broad-band, interstation measurements. Geophys. J. Int. 204, 517–534. https://doi.org/10.1093/gji/ggv462.
Souriau, A., Chevrot, S., Olivera, C., 2008. A new tomographic image of the Pyrenean lithosphere from teleseismic data. Tectonophysics 460, 206–214. https://doi.org/10.1016/j.tecto.2008.08.014.
Spakman, W., Wortel, R., 2004. A Tomographic View on Western Mediterranean Geodynamics. The TRANSMED Atlas. The Mediterranean Region from Crust to Mantle, pp. 31–52. https://doi.org/10.1007/978-3-642-18919-7_2.
Stehly, L., Fry, B., Campillo, M., Shapiro, N.M., Guilbert, J., Boschi, L., Giardini, D., 2009. Tomography of the Alpine region from observations of seismic ambient noise. Geophys. J. Int. 178, 338–350. https://doi.org/10.1111/j.1365-246X.2009.04132.x.
Teixell, A., Labaume, P., Ayarza, P., Espurt, N., Blanquat, M.D. Saint, Lagabrielle, Y., 2018. Tectonophysics Crustal structure and evolution of the Pyrenean-Cantabrian belt : a review and new interpretations from recent concepts and data. Tectonophysics 724–725, 146–170. https://doi.org/10.1016/j.tecto.2018.01.009.

Tesauro, M., Kaban, M.K., Cloetingh, S.A.P.L., 2008. EuCRUST-07: a new reference model for the European crust. Geophys. Res. Lett. 35. https://doi.org/10.1029/2007GL032244.
Udías, A., 2009. Jesuits' studies of earthquakes and seismological stations. Geol. Soc. Lond. Spec. Publ. 310, 135–143. https://doi.org/10.1144/SP310.16.
Van Eck, T., Trabant, C., Dost, B., Hanka, W., Giardini, D., 2004. Setting up a virtual broadband seismograph network across Europe. EoS Transactions 85, 125–129. https://doi.org/10.1029/2004EO130001.
Verbeke, J., Boschi, L., Stehly, L., Kissling, E., Michelini, A., 2012. High-resolution Rayleigh-wave velocity maps of Central Europe from a dense ambient-noise data set. Geophys. J. Int. 188, 1173–1187. https://doi.org/10.1111/j.1365-246X.2011.05308.x.
Vergés, J., Fernàndez, M., 2012. Tethys–Atlantic interaction along the Iberia – Africa plate boundary: The Betic–Rif orogenic system. Tectonophysics 576, 144–172. https://doi.org/10.1016/j.tecto.2012.08.032.
Villaseñor, A., Yang, Y., Ritzwoller, M.H., Gallart, J., 2007. Ambient noise surface wave tomography of the Iberian Peninsula: Implications for shallow seismic structure. Geophys. Res. Lett. 34, 1–5. https://doi.org/10.1029/2007GL030164.
Vinnik, L.P., Makeyeva, L.I., Milev, A., Usenko, A.Y., 1992. Global patterns of azimuthal anisotropy and deformations in the continental mantle. Geophys. J. Int. 433–447. https://doi.org/10.1111/j.1365-246X.1992.tb02102.x.
Vinnik, L.P., Krishna, V.G., Kind, R., Bormann, P., Stmmler, K., 1994. Shear wave splitting in the records of the German Regional Seismic Network. Geophys. Res. Lett. 21, 457–460. https://doi.org/10.1029/94GL00396.
Wessel, P., Smith, W.H.F., Scharroo, R., Luis, J., Wobbe, F., 2013. Generic mapping tools: improved version released. Eos 94, 409–410. https://doi.org/10.1002/2013EO450001.
Wilson, M., Downes, H., 2006. Tertiary-Quaternary Intra-Plate Magmatism and Mantle Dynamics in Europe. Geol. Soc. Lond. Mem. 32, 147–166. https://doi.org/10.1144/GSL.MEM.2006.032.01.09.
Winchester, J.A., Pharaoh, T.C., Verniers, J., 2002. Palaeozoic amalgamation of Central Europe: an introduction and synthesis of new results from recent geological and geophysical investigations. Geol. Soc. Lond. Spec. Publ. 201, 1–18. https://doi.org/10.1144/GSL.SP.2002.201.01.01.
Wortel, M.J.R., Spakman, W., 2000. Subduction and Slab Detachment in the Mediterranean-Carpathian Region. Science 290, 1910–1917. https://doi.org/10.1126/science.290.5498.1910.
Wüstefeld, A., Bokelmann, G., Barruol, G., Montagner, J.P., 2009. Identifying global seismic anisotropy patterns by correlating shear-wave splitting and surface-wave data. Phys. Earth Planet. Inter. 176, 198–212. https://doi.org/10.1016/j.pepi.2009.05.006.
Yang, Y., Ritzwoller, M.H., Levshin, A.L., Shapiro, N.M., 2007. Ambient noise Rayleigh wave tomography across Europe. Geophys. J. Int. 168, 259–274. https://doi.org/10.1111/j.1365-246X.2006.03203.x.
Zhang, Z., Karato, S., 1995. Lattice preferred orientation of olivine aggregates in simple shear. Nature 375, 774–777.
Zhang, X., Paulssen, H., Lebedev, S., Meier, T., 2009. 3D shear velocity structure beneath the Gulf of California from Rayleigh wave dispersion. Earth Planet. Sci. Lett. 279, 255–262. https://doi.org/10.1016/j.epsl.2009.01.003.
Zhu, H., Tromp, J., 2013. Mapping tectonic deformation in the crust and upper mantle beneath Europe and the North Atlantic Ocean. Science 341, 871–875. https://doi.org/10.1126/science.1241335.
Ziegler, P.A., 1982. Faulting and graben formation in western and Central Europe. Philosoph. Transac. - Royal Society of London, Series A 305, 113–143.
Ziegler, P.A., 1992. Plate tectonics, plate moving mechanisms and rifting. Tectonophysics 215, 9–34. https://doi.org/10.1016/0040-1951(92)90072-E.
Zielhuis, A., Nolet, G., 1994. Deep Seismic Expression of an Ancient Plate Boundary in Europe. Science 265, 79–81. https://doi.org/10.1126/science.265.5168.79.